Novel Electron Transport and Host Materials for Application to Organic Light-Emitting Diodes

富樫, 和法
九州大学大学院工学府物質創造工学専攻

https://doi.org/10.15017/26455

出版情報：九州大学, 2012, 博士（工学）, 課程博士
バージョン：
権利関係：

2013

Doctor Thesis

Novel Electron Transport and Host Materials for Application to Organic Light-Emitting Diodes

Kazunori Togashi

Department of Chemistry and Biochemistry

Graduate School of Engineering

Kyushu University

Table of contents

Chapter 1

Introduction

1-1. General introduction

In recent years, organic light-emitting diodes (OLEDs) have been attracting considerable attention because of their great potential for use in practical applications such as flat panel displays and lighting. The advanced characteristics of OLEDs have a large potential to replace the present LCD technologies. Advanced OLEDs[1,2] generally consist of organic multilayer structures containing hole transport layers (HTLs), emitting layer (EML) and electron transport layers (ETLs).[3,4] In the past 20 years, many kinds of electron transport materials (ETMs) have been developed along with hole transport materials (HTMs). Tris(8-hydroxyquinolinato)aluminum (Alq_3) which was firstly reported by Tang and co-workers of Eastman Kodak Co. is an excellent material as not only an EML but also ETL. Further, it can be an electron injection layer when it is combined with other EMLs. However, OLEDs' performance has been limited by the Alq_3's low electron mobility of 10^{-6} cm^2/Vs. Therefore, high performance ETMs instead of Alq_3 have been demanded to obtain lower power consumption of OLEDs. The physical properties requisite for ETM is summarized as below.

==========Requirements for ETMs==========

1. High electron affinity (E_a)
2. High electron mobility (μ_e)
3. Good amorphous property in a thin film state (high glass transition temperature (T_g))
4. Good thermal resistance
5. Electrochemical (oxidization and reduction) stability
6. High purity

==========

The requirement of No. 3-6 is a common issue for all materials in OLEDs, while No. 1 and 2 are requisite for ETMs.

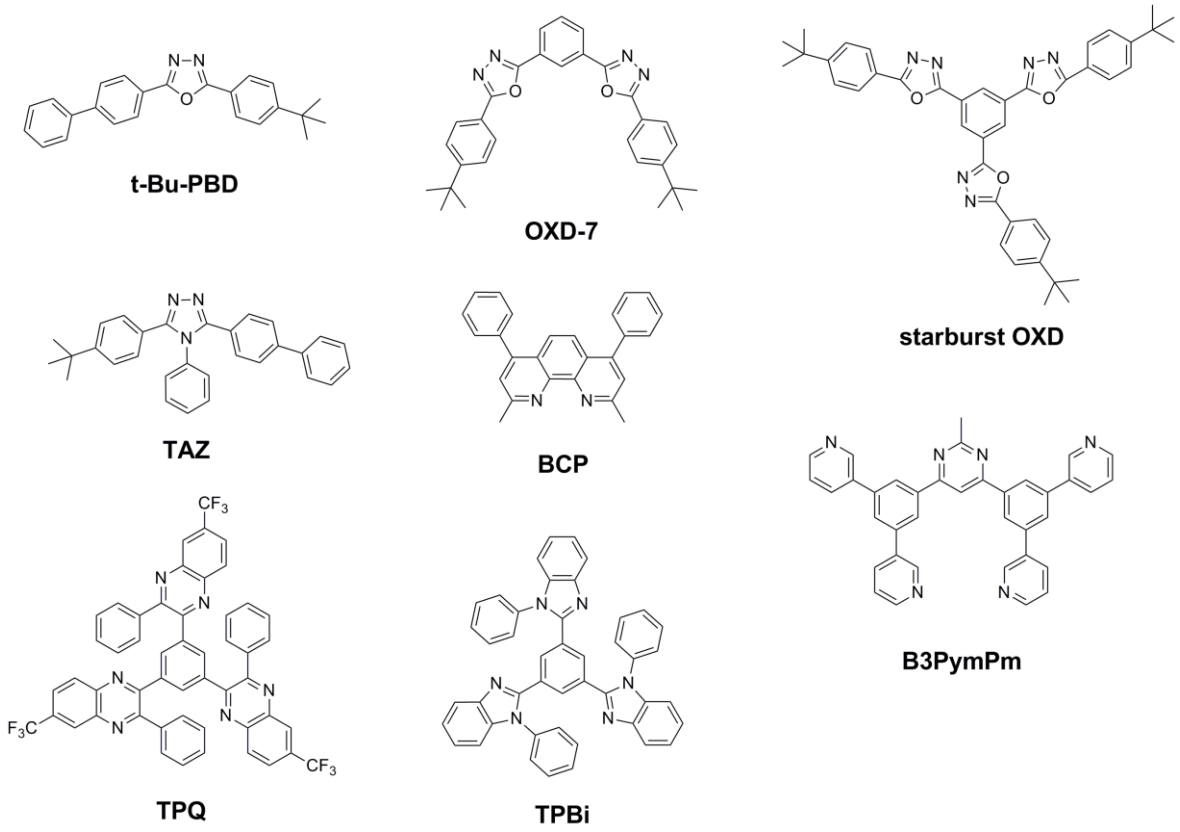

Figure 1-1. Chemical structures of typical ETMs.

Figure 1-1 shows chemical structures of typical ETMs. As ETMs except Alq_3, oxadiazole derivatives (OXDs) such as 2-([1,1'-biphenyl]-4-yl)-5-(4-tert-butylphenyl)-1,3,4-oxadiazole (t-Bu-PBD)[5] have been developed widely in the very early stage in the 1980s. Although t-Bu-PBD has good electron transport properties, it has been a problem in the device stability due to the lack of morphological and electrochemical stabilities. Then, in order to improve the thin film morphology of the amorphous state,

1,3-bis(5-(4-tert-butylphenyl)-1,3,4-oxadiazol-2-yl)benzene (OXD-7)[6] and 1,3,5-tris(5-(4-tert-butylphenyl)-1,3,4-oxadiazol-2-yl)benzene (starburst-type OXD)[7] have been developed. A triazole derivative 3-([1,1'-biphenyl]-4-yl)-5-(4-tert-butylphenyl)-4-phenyl-4H-1,2,4-triazole (TAZ)[8] has been also developed as an ETM having a structure similar to OXD. TAZ has high hole blocking properties in addition to electron transport properties because it has a relatively low-lying ionization potential (-6.6 eV). A phenanthroline derivative 2,9-dimethyl-4,7-diphenyl-1,10-phenanthroline (BCP)[9] also has a low-lying ionization potential (-6.7 eV) and high hole blocking properties like TAZ. Others, a phenylquinoxaline derivative 1,3,5-tris[(3-phenyl-6-trifluoromethyl)quinoxaline-2-yl]benzene (TPQ)[10] and a benzimidazole derivative 1,3,5-tris(1-phenyl-1H-benzo[d]imidazol-2-yl)benzene (TPBi)[11] have been reported, and they have high electron transport properties and good thin film stability. Also, it has been reported that a pyrimidine derivative 4,6-bis(3,5-di(pyridin-3-yl)phenyl)-2-methylpyrimidine (B3PymPm)[12] has a high triplet level and it is useful for phosphorescent organic light-emitting diodes (PHOLEDs). The ETMs which possess a higher triplet energy level (E_T) than that of host materials can prevent the leakage of triplet excitons, indicating that it can lead to the improvement of luminance efficiency in PHOLEDs. As shown in Fig. 1-1, a variety of the electron-withdrawing aromatic heterocycles was introduced into the molecular structures of ETMs since introducing an electron-withdrawing group causes the increase of E_a and makes easy to generate a radical anion. However, the introduction of an electron-withdrawing group will induce a large dipole moment, reducing μ_e.

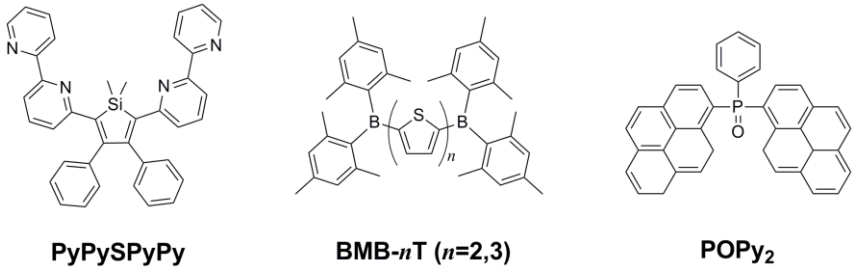

Figure 1-2. Chemical structures of ETMs having B and P=O elements as electron withdrawing groups.

Figure 1-2 shows chemical structures of the ETMs having other electron-withdrawing elements such as B and P=O, i.e., a silole derivative 6,6''-(1,1-dimethyl-3,4-diphenyl-1H-silole-2,5-diyl)di-2,2'-bipyridine (PyPySPyPy)[13], a boron derivative (BMB-nT (n= 2, 3))[14-16] and a phosphine oxide derivative phenyl-dipyrenylphosphine oxide ($POPy_2$)[17]. The silole backbone has a high E_a, without introducing an electron-withdrawing group. It has been predicted from the molecular orbital calculation that an E_a of silole derivatives can be deepened by the conjugation between the σ^* orbital of the silicon atom and the π^* orbital of the carbon atom (σ-π conjugation).[18] Further, it has been reported that the combination of two electron-donating pyrenes and an electron-accepting phosphine oxide provides good electron transport properties in $POPy_2$. In addition, it has been reported that an ETL formed by co-evaporation of $POPy_2$ and cesium is effective for lowering drive-voltage in OLEDs because the charge-transfer complex can be formed between them.

Next, I focus on μ_e which is one of fundamental requirements as ETMs in addition to E_a. In order to obtain high μ_e, densely packed intermolecular arrangement is required because it leads to large overlaps of π-orbitals contributing to efficient electron transport. Therefore, inducing horizontal molecular orientation to a substrate has been considered. In recent years,

it has been some reports in the horizontal orientation to a substrate by using unique molecules having planar and linear shaped structures to a substrate (Fig. 1-3).[19,20]

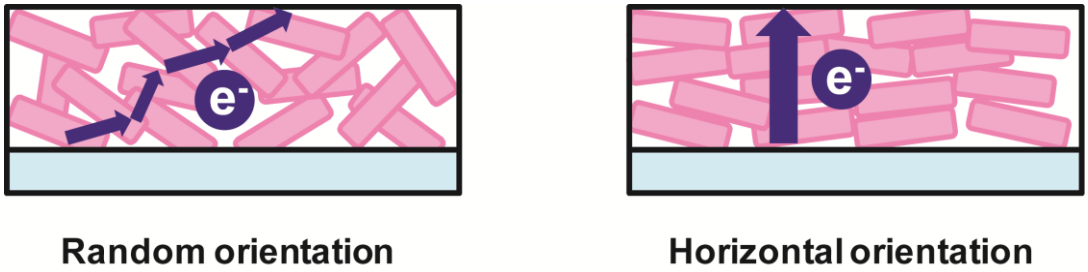

Figure 1-3. Schematic image of the random and horizontal orientations of linear shaped molecules in amorphous films.

Time of Flight (TOF) method has been widely used for measurements of μ_e. It has been revealed that the Alq_3 has a low μ_e of 1.2×10^{-6} cm^2/Vs which is much lower than the hole mobilities (10^{-3} cm^2/Vs) of the typical HTMs. Therefore, in recent years, ETMs with high μ_e have been developed to improve the carrier balance. It has been reported that the μ_e of B3PymPm, TPQ and PyPySiPyPy are about 10^{-5}, 10^{-4} and 10^{-4} cm^2/Vs, respectively.[12,13] Furthermore, it has been also reported that the μ_e of 1,3-bis(5-([2,2'-bipyridin]-6-yl)-1,3,4-oxadiazol-2-yl)benzene (Bpy-OXDm) (outlined in Fig. 1-4) is about 10^{-3} cm^2/Vs, approaching to the hole mobilities of the typical HTMs.[21] As shown in Fig. 1-4, the Bpy-OXDm has a hybrid molecular structure combined with the oxadiazole group having large E_a and the bipyridyl group having good electron stability. Generally, strong intermolecular interaction and small reorientation energy are required to obtain the high μ_e. It has been inferred that the planarity of the bipyridyl group and the delocalization of the lowest unoccupied molecular orbital (LUMO) from the oxadiazole ring to the pyridine ring make contribution to the high μ_e and E_a of Bpy-OXDm.[22] Also, Bpy-OXDm forms a

highly anisotropic film, indicating its planar molecular structure contributes horizontal orientation.[19] As a results, Bpy-OXDm shows more than 30 times higher μ_e than that of OXD-7, while the geometric and electronic structures of their main conformers are quite similar.[23]

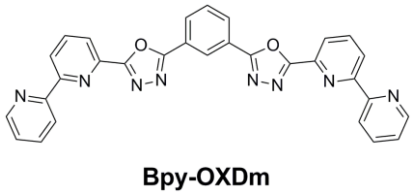

Figure 1-4. Chemical structure of Bpy-OXDm.

However, we have to pay attention that the TOF method has disadvantage. Since it requires thicker films over 1 μm, it is generally difficult to measure the mobilities for crystalline materials. Furthermore, the morphology of thin films around 100 nm thickness is significantly different from that of the thick film of around 1 μm. Therefore, it is sometimes inconsistent to assume that the thick films used in the TOF measurement have same film morphologies as in practical OLEDs. Thus, comparison of the *J-V* characteristics instead of the TOF measurement, the electron-only devices (EODs) is widely used for investigating electron transport properties of ETMs.

As shown in Fig. 1-1, 1-2 and 1-4, many kinds of molecular frames are introduced into ETMs, indicating that ETMs has a large freedom in their molecular structures. In recent years, the development of ETMs aimed for high efficiency and long lifetime and low driving voltage in OLEDs has been conducted.

In recent years, PHOLEDs have been intensively investigated to realize high luminance

efficiency because their internal quantum efficiency (η_{int}) can reach ≈100%, corresponding to an external quantum efficiency (η_{ext}) of about 20%. In contrast, η_{int} is limited to 25% in fluorescent OLEDs, corresponding to η_{ext} of ≈5%.[24] However, efficiency roll-off at high current density caused by triplet-triplet annihilation (TTA) of excitons is significant in PHOLEDs.[25-27] Improving the carrier balance in the EML and broadening the carrier recombination zone can suppress such efficiency roll-off at high current density.[28,29] Recently, bipolar phosphorescent (PH) host materials containing hole-transporting (donor) and electron-transporting (acceptor) moieties have been developed to improve the carrier balance in the EML (Fig. 1-5).[30-32] Further, PHOLEDs with double-emission layers have also been developed to broaden the carrier recombination zone.[28]

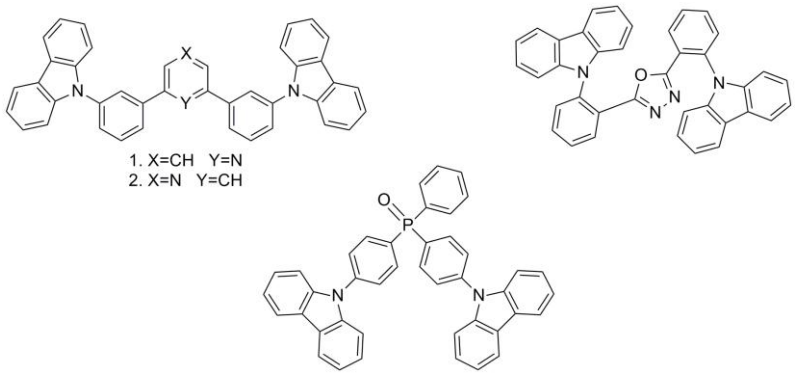

Figure 1-5. Chemical structures of PH host materials containing donor and acceptor moieties.

PH host materials need seven requirements as shown below. Especially, items No. 1-3 are necessary for PH host materials.

==========Requirements for PH host materials==========

1. High E_T level
2. Suitable HOMO and LUMO levels
3. High bipolar carrier transport properties
4. Good amorphous property in a thin film state (high T_g)
5. Good thermal resistance
6. Electrochemical (oxidization and reduction) stability
7. High purity

==========

To optimize device performance, PH host materials need to possess a higher E_T than that of guest emitters to confine triplet excitons in an EML. In order to design PH host materials with high E_T, it is necessary to consider the following point.

1. Introduction of molecular frames having rather short π conjugation
2. Introduction of twisted molecular structures to suppress planarity

E_T values of the typical condensed polycyclic aromatic units are summarized in Table 1-1.[33] As shown in Table 1-1, phenanthrene, triphenylene, dibenzofuran, dibenzothiophene and fluorene have high E_T compared to those of naphthalene, anthracene, pyrene and chrysene.

Further, host layers should have balanced carrier transport properties with appropriate highest occupied molecular orbital (HOMO) and LUMO levels. Finally, EMLs should have high T_g and good thermal stability.

Table 1-1. E_T values of typical condensed polycyclic aromatic units

Structure	E_T (eV)	Structure	E_T (eV)
	3.66eV		2.70eV
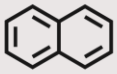	2.63eV		2.90eV
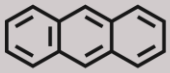	1.85eV	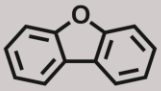	2.97eV
	2.11eV	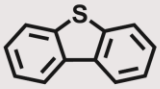	2.99eV
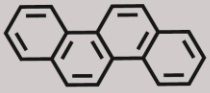	2.48eV	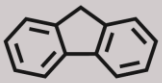	2.94eV

Figure 1-6 shows chemical structures of conventional PH host materials 4,4'-bis(carbazol-9-yl)-1,1'-biphenyl (CBP) and 1,3-bis(carbazol-9-yl)benzene (mCP). Although CBP and mCP have high E_T level 2.56 eV and 3.0 eV, respectively, they have rather low T_g (<100 °C) and their thin films can easily crystallize,[34-36] reducing device lifetime significantly.

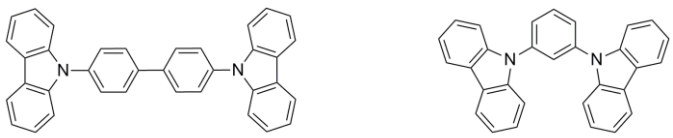

CBP mCP

Figure 1-6. Chemical structures of CBP and mCP.

1-2. Outline

In *Chapter 2*, I report the development of high performance triphenylene-based ETMs having a coplanar molecular structure with a large E_a for use in OLEDs. I discuss their molecular orientation and OLED characteristics.

In *Chapter 3*, I report molecular design aimed for higher horizontal molecular orientation of the ETMs having a long rod-like structure and their application as an ETM in OLEDs. I clarify the relationship between their molecular orientation and electron transport properties based on EODs and OLEDs.

In *Chapter 4*, I report the development of high performance triphenylene-based red PH host materials. I discuss their carrier transport properties based on hole-only devices (HODs) and EODs. Finally, I apply them as a host for red PHOLEDs.

1-3. References

1 J. L. Bredas, S. R. Marder and E. Reichmanis, *Chem. Mater.*, **2011**, 23, 309.

2 A. C. Grimsdale, K. L. Chan, R. E. Martin, P. G. Jokisz and A. B. Holmes, *Chem. Rev.*, **2009**, 109, 897.

3 C. W. Tang and S. A. VanSlyke, *Appl. Phys. Lett*., **1987**, 51, 913.

4 C. Adachi, T. Tsutsui and S. Saito, *Appl. Phys. Lett.*, **1990**, 57, 531.

5 C. Adachi, T. Tsutsui and S. Saito, *Appl. Phys. Lett.*, **1990**, 56, 799.

6 Y. Hamada, C. Adachi, T. Tsutsui and S. Saito, *J. Appl. Phys.*, **1992**, 31, 1812.

7 J. Bettenhausen, P. Strohriegl, W. Brutting, H. Tokuhisa and T. Tsutsui, *J. Appl. Phys.*, **1997**, 82, 4957.

8 J. Kido, C. Ohtaki, K. Hongawa, K. Okuyama and K. Nagai, *Jpn. J. Appl. Phys.*, **1993**, 32, L917.

9 V. I. Adamovich, S. R. Cordero, P. I. Djurovich, A. Tamayo, M. E. Thompson, B. W. D´Andrade and S. R. Forrest, *Org. Electron.*, **2003**, 4, 77.

10 M. Redecker, D. D. C. Bladley, M. Jandke and P. Strohriegl, *Appl. Phys. Lett.*, **1999**, 75, 109.

11 J. Shi, C. W. Tang and C. H. Chen, *U.S. Patent*, **1997**, No. 5646948.

12 D. Tanaka, H. Sasabe, Y.-J. Li, S.-J. Su, T. Takeda and J. Kido, *Jpn. J. Appl. Phys.*, **2007**, 46, L10.

13 K. Tamao, M. Uchida, T. Izumizawa, K. Furukawa and S. Yamaguchi, *J. Am. Chem. Soc.*, **1996**, 118, 11974.

14 M. Kinoshita and Y. Shirota, *Chem. Lett.*, **2001**, 7, 614.

15 A. J. Makinen, I. G. Hill, M. Kinoshita, T. Noda, Y.Shirota and Z. H. Kafafi, *J. Appl.*

Phys., **2002**, 91, 5456.

16 K. Okumoto, H. Kanno, Y. Hamada, H. Takahashi and K. Shibata, *J. Appl. Phys.*, **2006**, 100, 044507.

17 T. Oyamada, H. Sasabe, C. Adachi, S. Murase, T. Tominaga and C. Maeda, *Appl. Phys. Lett.*, **2005**, 86, 033503.

18 S. Yamaguchi and K. Tamao, *J. Chem. Soc. Dalton Trans.*, **1998**, 22, 3693.

19 D. Yokoyama, A. Sakaguchi, M. Suzuki and C. Adachi, *Appl. Phys. Lett.*, **2008**, 93, 173302.

20 D. Yokoyama, Y. Setoguchi, A. Sakaguchi, M. Suzuki and C. Adachi, *Adv. Funct. Mater.*, **2010**, 20, 386.

21 H. Murata, G. G. Malliaras, M. Uchida, Y. Shen and Z. H. Kafafi, *Chem. Phys. Lett.*, **2001**, 339, 161.

22 M. Ichikawa, N. Hiramatsu, N. Yokoyama, T. Miki, S. Narita, T. Koyama and Y. Taniguchi, *Phys. Stat. Sol. (RRL)*, **2007**, 1, R37.

23 D. Yokoyama, A. Sakaguchi, M. Suzuki and C. Adachi, *Appl. Phys. Lett.*, **2009**, 95, 243303.

24 C. Adachi, M. A. Baldo, M. E. Thompson and S. R. Forrest, *J. Appl. Phys.*, **2001**, 90, 5048.

25 M. A. Baldo, C. Adachi and S. R. Forrest, *Phys. Rev. B: Condens. Matter*, **2000**, 62, 10967.

26 C. Adachi, R. Kwong and S. R. Forrest, *Org. Electron.*, **2001**, 2, 37.

27 S. Reineke, K. Walzer and K. Leo, *Phys. Rev. B: Condens. Matter. Mater. Phys.*, **2007**, 75, 125328.

28 G. He, M. Pfeiffer and K. Leo, *Appl. Phys. Lett.*, **2004**, 85, 3911.

29 J. Lee, J.-I. Lee, J. Y. Lee and H. Y. Chu, *Appl. Phys. Lett.*, **2009**, 94, 193305.

30 S.-J. Su, H. Sasabe, T. Takeda and J. Kido, *Chem. Mater.*, **2008**, 20, 1691.

31 Y. Tao, Q. Wang, C. Yang, Q. Wang, Z. Zhang, T. Zou, J. Qin and D. Ma, *Angew. Chem. lnt. Ed.*, **2008**, 47, 8104.

32 H.-H. Chou and C.-H. Cheng, *Adv. Mater.*, **2010**, 22, 2468.

33 T. Horiuchi, J. Kamatani, N. Yamada, K. Kishino and A. Saitoh, *PCT Int. Appl.*, **2011**, WO 2011136156.

34 M.-H. Tsai, Y.-H. Hong, C.-H. Chang, H.-C. Su, C.-C. Wu, A. Matoliukstyte, J. Simokaitiene, S. Grigalevicius, J. V. Grazulevicius and C.-P. Hsu, *Adv. Mater.*, **2007**, 19, 862.

35 S.-J. Yeh, M.-F. Wu, C.-T. Chen, Y.-H. Song, Y. Chi, M.-H. Ho, S.-F. Hsu and C. H. Chen, *Adv. Mater.*, **2005**, 17, 285.

36 C.-L. Ho, W.-Y. Wong, Z.-Q. Gao, C.-H. Chen, K.-W. Cheah, B. Yao, Z. Xie, Q. Wang, D. Ma, L. Wang, X.-M. Yu, H.-S. Kwok and Z. Lin, *Adv. Funct. Mater.*, **2008**, 18, 319.

Chapter 2

Low Driving Voltage Characteristics of Triphenylene Derivatives as Electron Transport Materials in Organic Light-Emitting Diodes

2-1. Introduction

OLEDs have been attracting considerable attention because of their great potential for use in practical applications such as flat panel displays and lighting. Advanced OLEDs[1,2] generally consist of organic multilayer structures containing hole transport, emitting, and electron transport layers (ETLs).[3,4] Balanced charge carrier recombination is required to achieve high efficiency, but the hole mobilities are usually much higher than the μ_e in OLEDs.[5,6] Although many kinds of ETM have been developed,[7-14] Alq_3 is still the most widely used ETM. Despite its rather low μ_e of 10^{-6} cm^2/Vs,[15] Alq_3 has relatively good durability under continuous operation. Since the initial discovery of oxadiazole derivatives for use as ETMs,[16] these compounds have been developed extensively, and oxadiazole derivatives with high μ_e and E_a[17,18] have recently attracted a great deal of attention. However, the lifetimes of OLEDs containing oxadiazole-based compounds are rather short compared with those of devices using Alq_3. The development of ETMs with both high μ_e and durability therefore remains an important challenge.

Although the developmental progress of blue luminescent materials[19-22] has been remarkable, blue OLEDs tend to promote increased degradation of the proximate ETL in comparison with red and green OLEDs, because the excitonic energy generated in the EML is higher. Therefore, there are really very few stable ETMs available for use in blue OLEDs.

Here, I report the development of novel ETMs based on a triphenylene frame. I have clarified the electron transport properties of these ETMs and measured the lifetimes of blue OLEDs using them as ETLs.

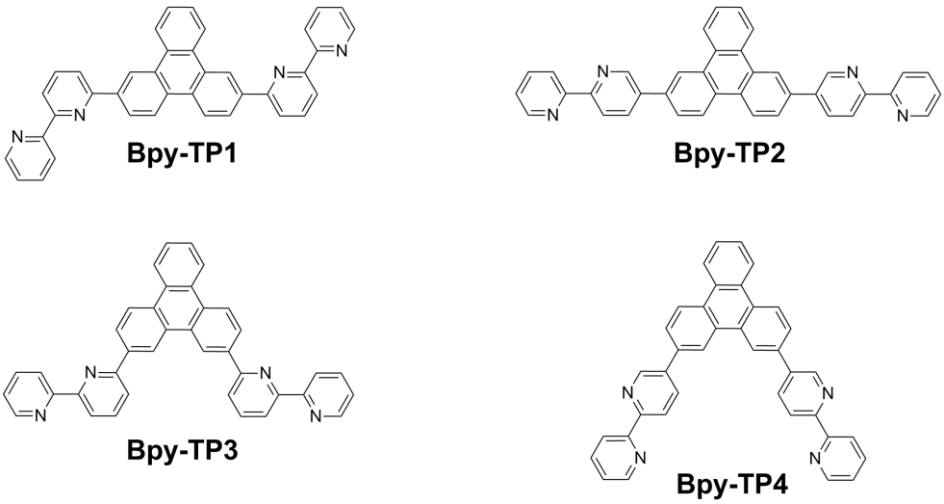

Figure 2-1. Chemical structures of Bpy-TP1-4.

2-2. Experimental section

The chemical structures of the four newly developed materials, Bpy-TP1, Bpy-TP2, Bpy-TP3 and Bpy-TP4, are shown in Fig. 2-1. The materials were synthesized by the Suzuki-Miyaura coupling reaction[23,24] and were then purified by sublimation before characterization.

Synthesis

The synthesis route used to obtain Bpy-TP1 and Bpy-TP2 is outlined in Scheme 2-1. 3,3''-Bis(trimethylsilyl)-1,1':2',1''-terphenyl (**5**), 3,3''-dibromo-1,1':2',1''-terphenyl (**6**) and 2,7-dibromotriphenylene (**7**) were prepared according to procedures described in the literature.[25]

The procedure developed to synthesize Bpy-TP3 and Bpy-TP4 is shown in Scheme 2-2. 1,2-Bis(4,4,5,5,-tetramethyl-[1,3,2]dioxaborolan-2-yl)benzene (**9**),[26] 2,2'-dibromo-3,3'-dimethoxy-1,1'-biphenyl (**10**)[27] and 2,11-Dimethoxytriphenylene (**11**)[28] were prepared according to previously reported procedures.

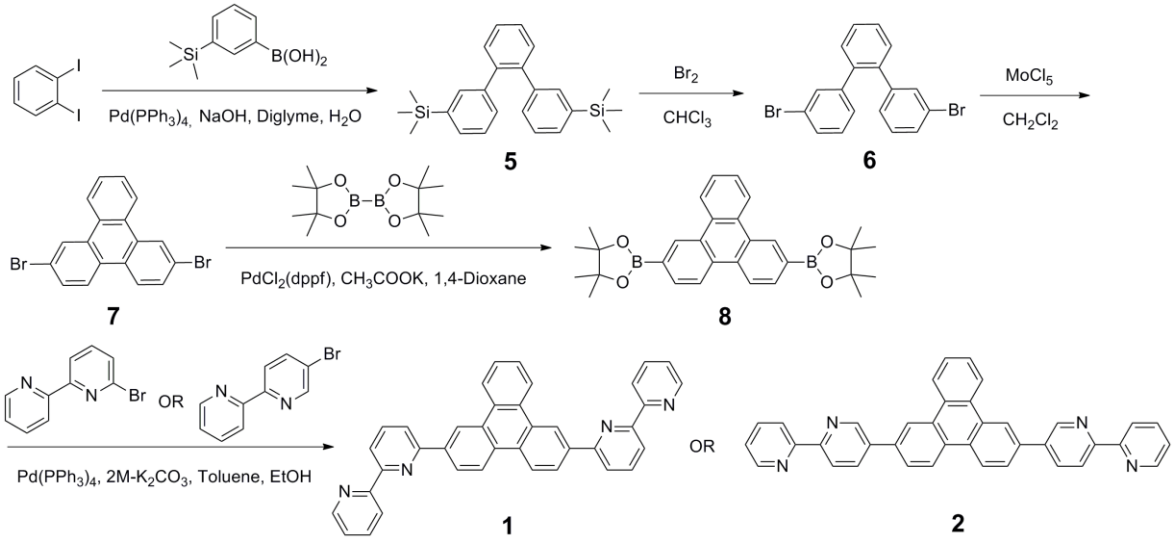

Scheme 2-1. Synthesis route for Bpy-TP1 (**1**) and Bpy-TP2 (**2**).

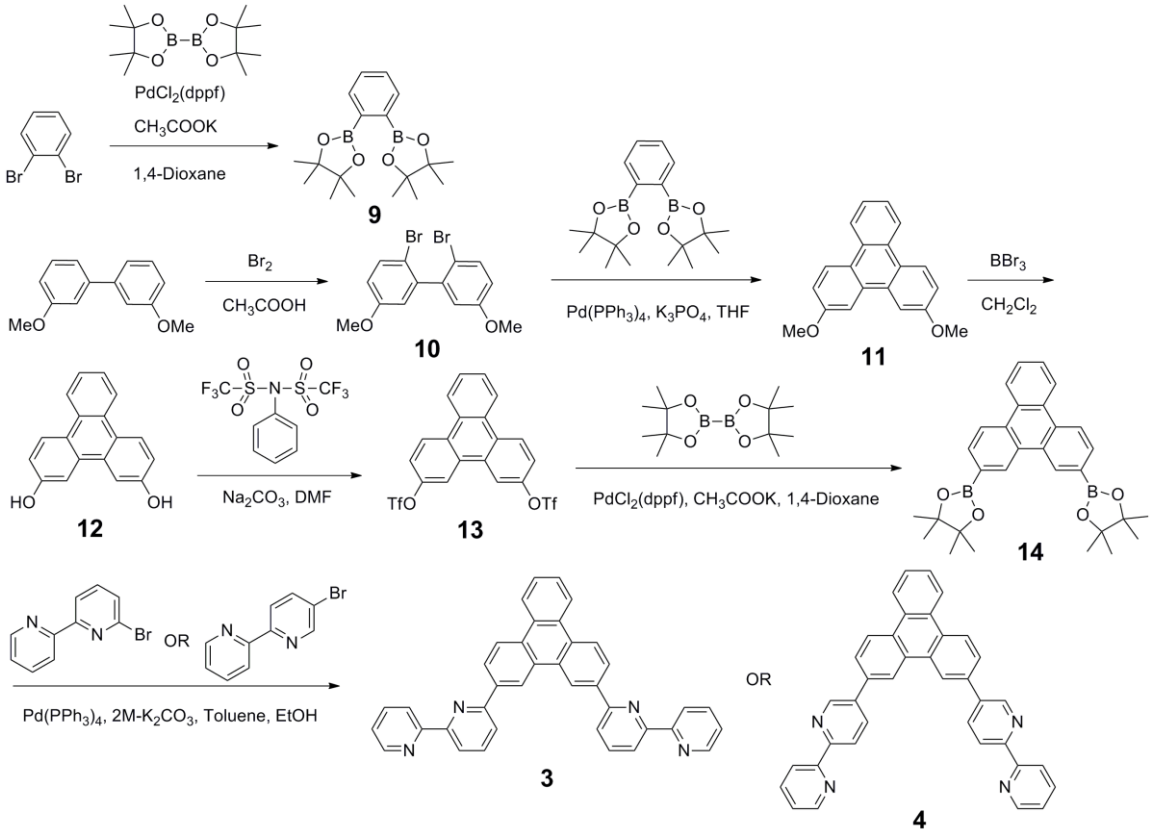

Scheme 2-2. Synthesis route for Bpy-TP3 (**3**) and Bpy-TP4 (**4**).

*(**5**) 3,3''-Bis(trimethylsilyl)-1,1':2',1''-terphenyl*

A mixture of 1,2-diiodobenzene (73.8 mmol), 3-trimethylsilylboronic acid (155 mmol), tetrakis(triphenylphosphine)palladium(0) (3.7 mmol), NaOH (221 mmol), diethyleneglycol dimethyl ether (160 mL) and water (40 mL) was added to a flask. The mixture was degassed and then heated under reflux for 15 h under a nitrogen atmosphere. The mixture was then cooled to room temperature and the solvent was removed by distillation. The crude product was extracted using toluene, dried using $MgSO_4$, filtered to remove any precipitates, and then distilled to remove any solvents. Purification by column chromatography on silica gel with *n*-hexane and washing with methanol yielded a white powder. Yield: 84%. ^{1}H NMR (600 MHz, $CDCl_3$, TMS): δ (ppm) 0.0 (18H, s), 7.06 (2H, s), 7.20 (4H, m), 7.26 (2H, dd, *J*=4.8 Hz), 7.38 (2H, m), 7.42 (2H, m).

*(**6**) 3,3''-Dibromo-1,1':2',1''-terphenyl*

A mixture of **5** (61.4 mmol) and chloroform (90 mL) was added to a flask and cooled to -5 °C. A solution of Br_2 (246 mmol) in chloroform (90 mL) was then added. The mixture was allowed to warm up to room temperature and was then stirred for 24 h. Saturated aqueous Na_2SO_3 (90 mL) was added to the mixture and stirred for 30 min. The crude product was extracted using chloroform, dried using $MgSO_4$, filtered to remove any precipitates, and then distilled to remove the solvent. Purification by washing with ethanol and methanol yielded a white powder. Yield: 65%. ^{1}H NMR (600 MHz, $CDCl_3$, TMS): δ (ppm) 6.97 (2H, d, *J*=7.2 Hz), 7.06 (2H, t, *J*=7.2 Hz), 7.36 (4H, m), 7.40 (2H, m), 7.43 (2H, m).

*(**7**) 2,7-Dibromotriphenylene*

A mixture of **6** (30.9 mmol), molybdenum(V) chloride (61.8 mmol) and dichloromethane (20 mL) was added to a flask and then stirred at room temperature for 19 h. Water (100 mL) was added to the mixture, which was stirred for 30 min. Then dichloromethane was removed by distillation and filtered. Chloroform (200 mL), *n*-hexane (600 mL) and SiO_2 (36.6 g) were added and the crude was dissolved at 60 °C. The solution was cooled to room temperature and then filtered to remove any precipitates. The solvent was removed by distillation to leave a crude pale yellow powder. Purification by washing with chloroform yielded a pale yellow powder. Yield: 46%. ^{1}H NMR (600 MHz, $CDCl_3$, TMS): δ (ppm) 7.66 (2H, m), 7.70 (2H, dd, *J*=9.0 Hz), 8.36 (2H, d, *J*=9.0 Hz), 8.49 (2H, m), 8.69 (2H, s).

***(8)** 2,7-Bis(4,4,5,5-tetramethyl-1,3,2-dioxaborolan-2-yl)triphenylene (2,7-BTMDT)*

A mixture of **7** (14.2 mmol), bis(pinacolato)diboron (31.2 mmol), [1,1'-bis(diphenylphosphino)ferrocene]dichloropalladium(II) (0.4 mmol), CH_3COOK (42.6 mmol) and 1,4-dioxane (50 mL) was added to a flask. The mixture was degassed and then stirred at 80 °C for 10 h under a nitrogen atmosphere. The mixture was then cooled to room temperature and filtered. Purification by washing with methanol produced an off-white powder. Yield: 70%. ^{1}H NMR (400 MHz, $CDCl_3$, TMS): δ (ppm) 1.43 (24H, s), 7.78 (2H, m), 8.05 (2H, d, *J*=8.1 Hz), 8.83 (4H, m), 9.16 (2H, s).

***(1)** 2,7-Bis(2,2'-bipyridine-6-yl)triphenylene (Bpy-TP1)*

A mixture of **8** (4.8 mmol), 6-bromo-2,2'-bipyridine (10.1 mmol), tetrakis(triphenylphosphine)palladium(0) (0.2 mmol), aqueous K_2CO_3 (2.0 M, 7.4 mL), toluene (40 mL) and ethanol (10 mL) was added to a flask. The mixture was degassed and

then heated under reflux for 9 h under a nitrogen atmosphere. The mixture was then cooled to room temperature and filtered. THF (1300 mL) was added, and the solid was dissolved at 60 °C. The solution was cooled to 40 °C and then filtered to remove the Pd catalyst. The solvent was removed by distillation to leave a crude pale yellow powder. Recrystallization from *o*-dichlorobenzene yielded Bpy-TP1 as a pale yellow powder. Yield: 66%. Melting point (Mp): 285 °C. IR (KBr): *v*=3057, 3011, 1610, 1580, 1561, 1505, 1470, 1458, 1443, 1419, 1388, 1313, 1265, 1222, 1183, 1169, 1153, 1104, 1092, 822, 800, 774, 761, 741, 705, 646, 635, 620, 579, 488, 419 cm^{-1}. UV/Vis (CH_2Cl_2): λ_{max}=279 nm. ^1H NMR (400 MHz, DMSO d-6): δ (ppm) 7.49 (2H, m), 7.81 (2H, m), 8.04 (2H, t, *J*=8.0 Hz), 8.12 (2H, t, *J*=8.0 Hz), 8.41 (2H, d, *J*=7.7 Hz), 8.45 (2H, d, *J*=7.7 Hz), 8.64 (2H, d, *J*=8.0 Hz), 8.70 (4H, m), 9.01 (2H, d, *J*=8.8 Hz), 9.08 (2H, m), 9.56 (2H, s). Elemental analysis: found C, 84.97%; H, 4.37%; N, 10.38%; calc. for $C_{38}H_{24}N_4$: C, 85.05%, H, 4.51%; N, 10.44%; MS (MALDI-TOF): *m*/*z* 537.18 $[M]^{+\cdot}$.

*(**2**) 2,7-Bis(2,2'-bipyridine-5-yl)triphenylene (Bpy-TP2)*

A mixture of **8** (5.0 mmol), 5-bromo-2,2'-bipyridine (10.5 mmol), tetrakis(triphenylphosphine)palladium(0) (0.3 mmol), aqueous K_2CO_3 (2.0 M, 7.7 mL), toluene (40 mL), and ethanol (10 mL) was mixed in a flask. The mixture was degassed and then heated under reflux for 9 h under a nitrogen atmosphere. The mixture was cooled to room temperature and then filtered. Chloroform (1300 mL) and SiO_2 (11.5 g) were added to the mixture, which was then stirred at 60 °C. The solution was then cooled to 40 °C and filtered to remove the precipitate. Removal of the solvent by distillation produced a crude pale yellow powder. Recrystallization from *o*-dichlorobenzene yielded Bpy-TP2 as a yellow

powder. Yield: 60%. Mp: 338 °C. IR (KBr): *v*=3052, 1612, 1589, 1573, 1486, 1462, 1437, 1365, 1281, 1246, 1146, 1092, 1070, 1040, 1024, 1004, 938, 871, 849, 791, 759, 703, 620, 419 cm^{-1}. UV/Vis (CH_2Cl_2): λ_{max}=343 nm. ^1H NMR (400 MHz, DMSO d-6): δ (ppm) 7.42 (2H, m), 7.72 (2H, m), 7.93 (2H, t, *J*=7.7 Hz), 8.12 (2H, d, *J*=8.4 Hz), 8.42 (2H, d, *J*=7.7 Hz), 8.50 (4H, m), 8.67 (2H, d, *J*=4.0 Hz), 8.94 (2H, d, *J*=8.8 Hz), 9.04 (2H, m), 9.16 (2H, s), 9.28 (2H, s). Elemental analysis: found C, 85.20%; H, 4.43%; N, 10.48%; calc. for $C_{38}H_{24}N_4$: C, 85.05%, H, 4.51%; N, 10.44%; MS (MALDI-TOF): *m*/*z* 537.18 $[M]^{+\cdot}$.

*(**10**) 2,2'-Dibromo-5,5'-dimethoxy-1,1'-biphenyl*

A mixture of 3,3'-dimethoxy-1,1'-biphenyl (140 mmol), bromine (308 mmol), and acetic acid (250 mL) was stirred at room temperature for 2 h. Saturated aqueous Na_2SO_3 (90 mL) was added and the mixture was stirred for 30 min. The crude product was extracted using chloroform, dried using $MgSO_4$, filtered to remove any precipitates, and then distilled to remove any solvents. Purification by washing with ethanol yielded a white powder. Yield: 70%. ^1H NMR (400 MHz, $CDCl_3$, TMS): δ (ppm) 3.12 (6H, s), 6.79 (2H, s), 6.81 (2H, dd, *J*=8.0 Hz), 7.53 (2H, d, *J*=8.0 Hz).

*(**11**) 2,11-Dimethoxytriphenylene*

A mixture of **10** (7.6 mmol), 1,2-bis(4,4,5,5-tetramethyl-1,3,2-dioxaborolan-2-yl)benzene (9.1 mmol), K_3PO_4 (45.5 mmol), tetrakis(triphenylphosphine)palladium(0) (0.4 mmol), THF (50 mL), and water (15 mL) was added to a flask. The mixture was degassed and then heated under reflux for 48 h under a nitrogen atmosphere. The mixture was then cooled to room temperature. The crude powder was extracted using chloroform, dried using $MgSO_4$, filtered

to remove any precipitates, and then distilled to remove any solvents. Purification by column chromatography on silica gel with a 1/10/1 (=v/v/v) ethyl acetate/*n*-hexane/dichloromethane mixture produced a white powder. Yield: 66%. ^{1}H NMR (400 MHz, $CDCl_3$, TMS): δ (ppm) 4.03 (6H, s), 7.28 (2H, dd, *J*=8.8 Hz), 7.57 (2H, dd, *J*=6.2 Hz), 7.96 (2H, s), 8.56 (2H, d, *J*=8.8 Hz), 8.67 (2H, dd, *J*=6.2 Hz).

*(**12**) Triphenylene-2,11-diol*

A mixture of **11** (5.2 mmol) and dichloromethane (50 mL) was added to a flask and cooled to -78 °C. A solution of BBr_3 in dichloromethane (1 mol/L, 10.9 mmol) was then added. The mixture was allowed to warm up to room temperature and was then stirred for 24 h. Water (100 mL) was added to the mixture, which was stirred for 30 min, and was then filtered. Purification by washing with methanol yielded a white powder. Yield: 93%. ^{1}H NMR (400 MHz, DMSO d-6): δ (ppm) 7.11 (2H, dd, *J*=8.8 Hz), 7.48 (2H, m), 7.76 (2H, s), 8.52-8.54 (4H, m), 9.88 (2H, s).

*(**13**) 2,11-Bis(trifluoromethanesulfonate)triphenylene*

A mixture of **12** (4.8 mmol), *N*-phenyl-bis(trifluoro-methanesulfonimide) (19.2 mmol), Na_2CO_3 (48 mmol) and dimethylformamide (50 mL) was degassed and was then stirred at room temperature for 12 h. Water (100 mL) was added to the mixture, which was stirred for 30 min, and then filtered. Purification by washing with methanol yielded a white powder. Yield: 91%. ^{1}H NMR (400 MHz, $CDCl_3$, TMS): δ (ppm) 7.64 (2H, dd, *J*=9.2 Hz), 7.76 (2H, m), 8.34 (2H, s), 8.62 (2H, m), 8.75 (2H, d, *J*=9.2 Hz).

*(**14**) 2,11-Bis(4,4,5,5-tetramethyl-1,3,2-dioxaborolan-2-yl)triphenylene (2,11-BTMDT)*

A mixture of **13** (4.4 mmol), bis(pinacolato)diboron (9.7 mmol), [1,1'-bis(diphenylphosphino)ferrocene]dichloropalladium(II) (0.13 mmol), CH_3COOK (13.2 mmol) and 1,4-dioxane (50 mL) was added to a flask. The mixture was degassed and was then stirred at 80 °C for 12 h under a nitrogen atmosphere. The mixture was then cooled to room temperature. The crude product was extracted using chloroform, filtered, and then distilled to remove any solvents. Purification by column chromatography on silica gel with a 1/5 (=v/v) ethyl acetate/*n*-hexane mixture yielded a white powder. Yield: 52%. ^{1}H NMR (400 MHz, $CDCl_3$, TMS): δ (ppm) 1.44 (24H, s), 7.67 (2H, m), 8.07 (2H, d, *J*=8.0 Hz), 8.63-8.70 (4H, m), 9.23 (2H, s). ^{13}C NMR (400 MHz, $CDCl_3$, TMS): δ (ppm) 133.01, 132.02, 130.64, 130.23, 129.26, 127.60, 123.71, 122.36, 84.07, 24.99. Elemental analysis: found C, 74.77%; H, 6.93%; calc. for $C_{30}H_{34}B_2O_4$: C, 75.03%, H, 7.14%; MS (MALDI-TOF): *m*/*z* 480.33 $[M]^{+\cdot}$.

*(**3**) 2,11-Bis(2,2'-bipyridine-6-yl)triphenylene (Bpy-TP3)*

A mixture of **14** (1.6 mmol), 6-bromo-2,2'-bipyridine (3.27 mmol), tetrakis(triphenylphosphine)palladium(0) (0.08 mmol), aqueous K_2CO_3 (2.0 M, 2.3 mL), toluene (40 mL) and ethanol (10 mL) was added to a flask. The mixture was degassed and then heated under reflux for 12 h under a nitrogen atmosphere. The mixture was cooled down to room temperature and then filtered. Recrystallization from *o*-dichlorobenzene yielded Bpy-TP3 as a pale yellow powder. Yield: 71%. Mp: 312 °C. IR (KBr): *v*=3060, 1581, 1562, 1468, 1448, 1429, 1417, 1394, 1318, 1269, 1164, 1146, 1092, 1042, 990, 909, 900, 874, 812, 779, 762, 740, 717, 683, 650, 622, 554, 490, 420 cm^{-1}. UV/Vis (CH_2Cl_2): λ_{max}=282 nm. ^{1}H NMR (400 MHz, DMSO d-6): δ (ppm) 7.42 (2H, t, *J*=5.9 Hz), 7.77 (4H, m), 8.15 (2H, d,

J=7.0 Hz), 8.41 (2H, d, *J*=7.0 Hz), 8.48 (2H, d, *J*=7.3 Hz), 8.63 (4H, d, *J*=4.8 Hz), 8.70 (2H, d, *J*=4.8 Hz), 8.89 (2H, m), 8.98 (2H, d, *J*=8.8 Hz), 9.74 (2H, s). Elemental analysis: found C, 84.87%; H, 4.51%; N, 10.46%; calc. for $C_{38}H_{24}N_4$: C, 85.05%, H, 4.51%; N, 10.44%; MS (MALDI-TOF): *m*/*z* 537.34 $[M]^{+\cdot}$.

*(**4**) 2,11-Bis(2,2'-bipyridine-5-yl)triphenylene (Bpy-TP4)*

A mixture of **14** (1.9 mmol), 5-bromo-2,2'-bipyridine (4.0 mmol), tetrakis(triphenylphosphine)palladium(0) (0.1 mmol), aqueous K_2CO_3 (2.0 M, 2.9 mL), toluene (40 mL) and ethanol (10 mL) was added to a flask. The mixture was degassed and heated under reflux for 12 h under a nitrogen atmosphere. The mixture was then cooled down to room temperature and filtered. Chloroform (1000 mL) and SiO_2 (11.5 g) were then added and this mixture was stirred at 60 °C in a flask. The solution was cooled down to 40 °C and filtered to remove any precipitates. The solvent was removed by distillation to yield a crude powder. Recrystallization from *o*-dichlorobenzene yielded Bpy-TP4 as a yellow powder. Yield: 63%. Mp: 351 °C. IR (KBr): *v*=3052, 3006, 1610, 1588, 1573, 1550, 1481, 1460, 1435, 1409, 1368, 1277, 1244, 1145, 1091, 1069, 1039, 1018, 1003, 993, 856, 818, 795, 763, 745, 720, 640, 618, 592, 419 cm^{-1}. UV/Vis (CH_2Cl_2): λ_{max}=310 nm. ^1H NMR (400 MHz, DMSO d-6): δ (ppm) 7.45 (2H, m), 7.74 (2H, m), 7.97 (2H, m), 8.16 (2H, dd, *J*=8.8 Hz), 8.46 (2H, d, *J*=7.7 Hz), 8.53 (2H, d, *J*=8.1 Hz), 8.59 (2H, d, *J*=6.2 Hz), 8.71 (2H, d, *J*=4.0 Hz), 8.87 (2H, d, *J*=3.3 Hz), 8.96 (2H, d, *J*=8.8 Hz), 9.37 (2H, s), 9.41 (2H, s). Elemental analysis: found C, 85.03%; H, 4.46%; N, 10.42%; calc. for $C_{38}H_{24}N_4$: C, 85.05%, H, 4.51%; N, 10.44%; MS (MALDI-TOF): *m*/*z* 536.31 $[M]^{+\cdot}$.

2-3. Results and discussion

Triphenylene-based ETMs with a coplanar molecular structure and a large E_a were designed to maximize their electron transport characteristics. Our concept is based on two fundamental ideas: that the planar triphenylene core will provide good electron transport ability and that the bipyridine unit will provide good electron injection ability because of its electron accepting characteristics. The planar structure of triphenylene is also advantageous for the induction of molecular orientation. To increase the E_a of the triphenylene-based aromatic hydrocarbons, we attached two bipyridine moieties at the 2 and 7 or 2 and 11 positions. The synthesis routes to the new triphenylene-based ETMs are shown in Schemes 2-1 and 2-2 in the experimental section.

The crude ETMs were sublimed, and their thermophysical properties were measured by differential scanning calorimetry (DSC). Their optical and photophysical properties were also evaluated by photoelectron spectroscopy (AC-3), ultraviolet-visible (UV-Vis) absorption and photoluminescence (PL) spectroscopies. Figure 2-2 shows UV-vis absorption and PL spectra of the synthesized ETMs in dichloromethane solution and neat films. The molecular orientations of the synthesized ETMs were evaluated by variable-angle spectroscopic ellipsometry (VASE) measurements. The film morphologies were measured by atomic force microscopy (AFM) and X-ray diffraction (XRD). The UV-Vis absorption and PL properties of these films deposited on a quartz substrate are summarized in Table 2-1.[29] None of the triphenylene-based ETMs exhibited a glass transition temperature (T_g) in the DSC measurements.

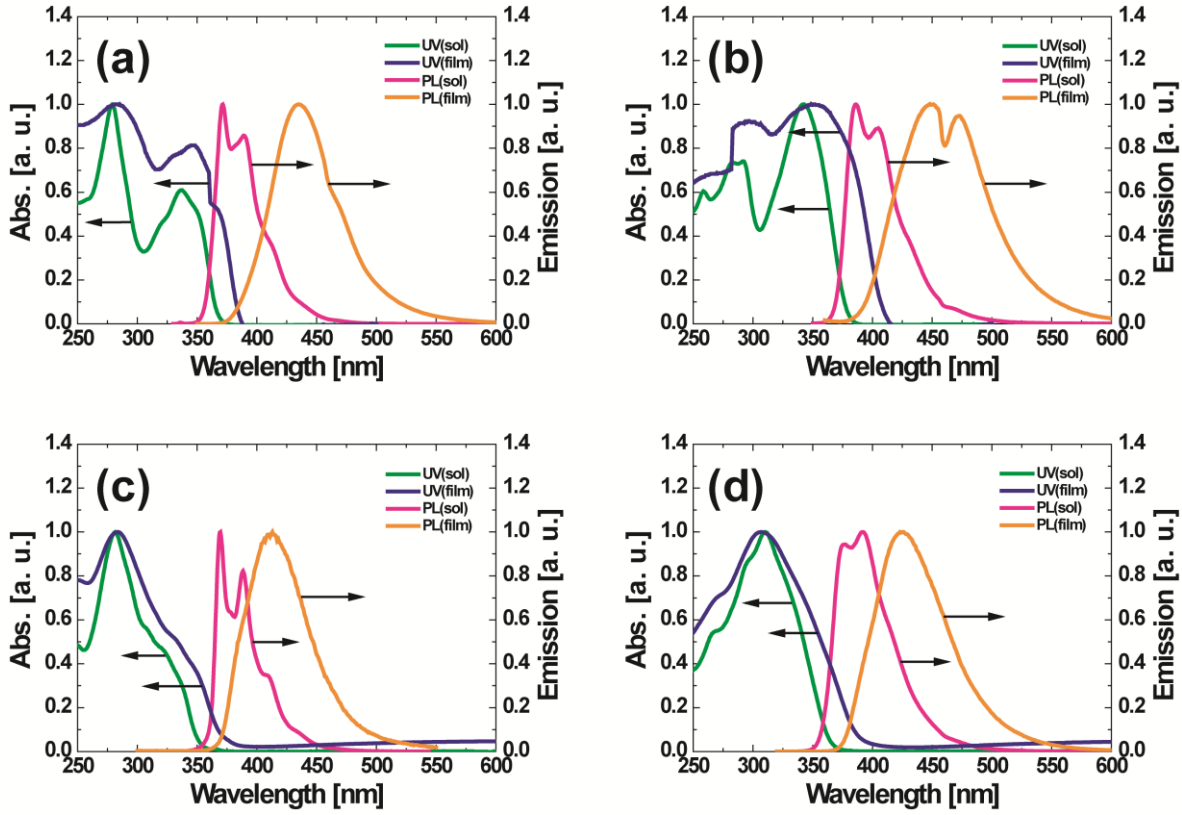

Figure 2-2. UV-vis absorption and PL spectra of (a) Bpy-TP1, (b) Bpy-TP2, (c) Bpy-TP3 and (d) Bpy-TP4 in dichloromethane solution and neat films.

Table 2-1. Physical properties of triphenylene-based ETMs

	T_m [a] (°C)	T_g [b] (°C)	E_g [c] (eV)	I_p [d] (eV)	I_p [e] (eV)	E_a [f] (eV)	E_a [g] (eV)
Bpy-TP1	285	N.O.	3.2	-5.6	-5.7	-1.6	-2.5
Bpy-TP2	338	N.O.	3.0	-5.7	-5.7	-1.8	-2.7
Bpy-TP3	312	N.O.	3.4	-5.7	-5.7	-1.5	-2.3
Bpy-TP4	351	N.O.	3.3	-5.7	-5.8	-1.7	-2.5

[a] Melting point. [b] Glass transition temperature. [c] Energy gap estimated from the absorption edge of the films. [d] Ionization potential obtained by DFT (B3LYP/6-31G) calculation. [e] Ionization potential determined by AC-3 measurements. [f] Electron affinity obtained by DFT (B3LYP/6-31G) calculation. [g] Electron affinity estimated from the difference between I_p [e] and E_g [c].

However, as shown in Fig. 2-3, the XRD spectra of all of the vacuum-deposited thin films of these ETMs showed that they had amorphous morphologies. AFM observation of the vacuum-deposited ETM thin films also showed that they had smooth surfaces with low surface roughness, as shown in the inset of Fig. 2-3.

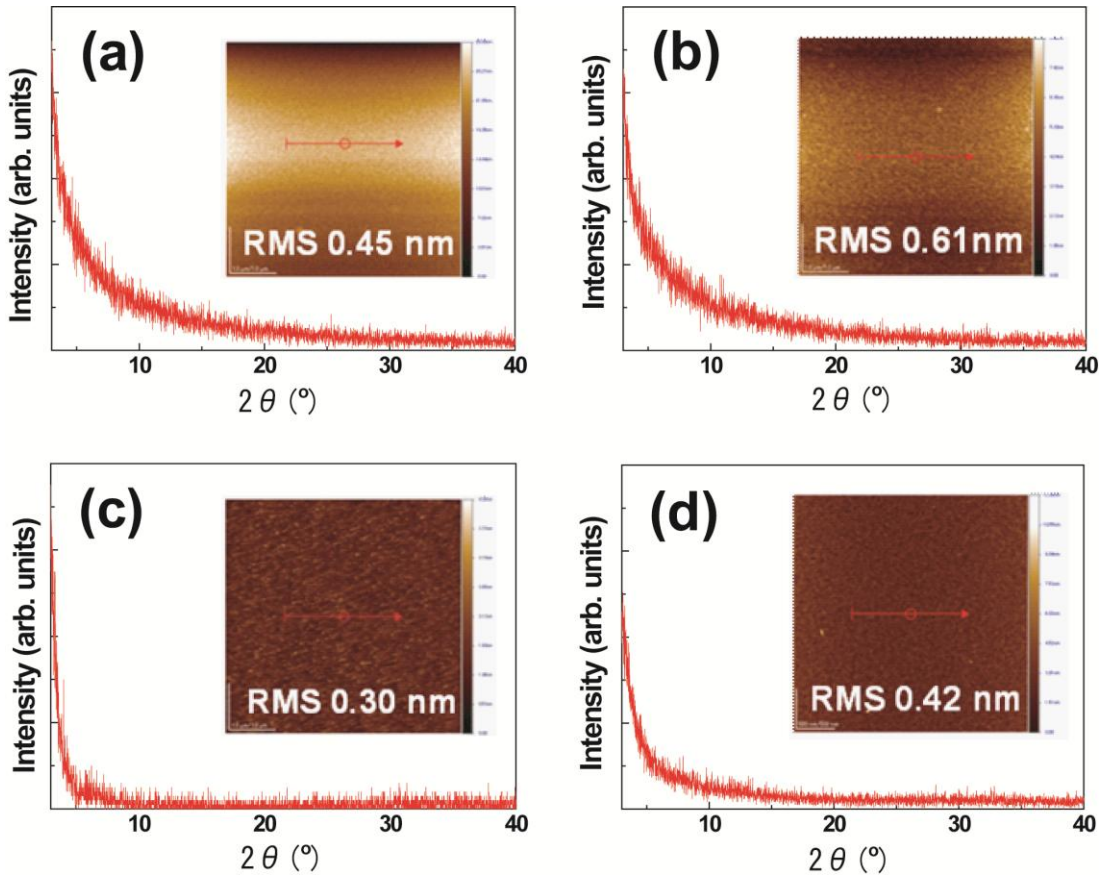

Figure 2-3. XRD spectra of vacuum-deposited thin films of (a) Bpy-TP1, (b) Bpy-TP2, (c) Bpy-TP3 and (d) Bpy-TP4. Insets: AFM images of the thin films.

The molecular orientation of the films was investigated using VASE analysis. From the VASE results, I can quantify the molecular orientation of each of the amorphous films using the orientation parameter S, where

$$S = \frac{k_e - k_o}{k_e + 2k_o} \qquad (2-1)$$

where k_o and k_e are the ordinary and extraordinary extinction coefficients at the wavelength of maximum absorption, respectively. If the molecules are aligned such that they are completely parallel to the surface, S=-0.5; if they are randomly oriented, S=0; and if they are completely perpendicular to the surface, S=1.[30] As shown in Fig. 2-4, the values of S determined from the VASE analysis are -0.2 for Bpy-TP1, -0.1 for Bpy-TP2 and Bpy-TP4, and +0.1 for Bpy-TP3. Therefore, the triphenylene-based ETMs, apart from Bpy-TP3, have optical anisotropy and tend to be oriented parallel to the Si substrate in their deposited amorphous thin film forms.

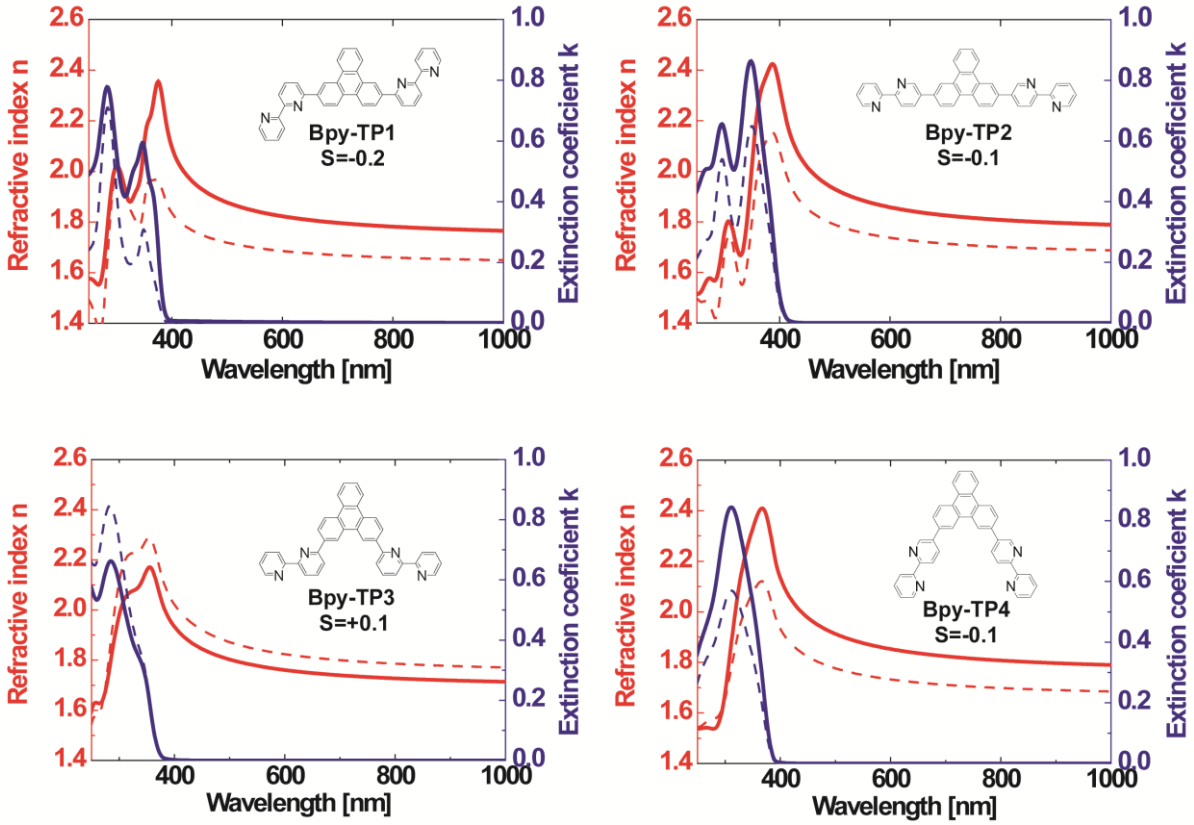

Figure 2-4. Refractive indices (red) and extinction coefficients (blue) of synthesized ETMs. The solid and broken lines indicate the ordinary and extraordinary components of the optical constants, respectively.

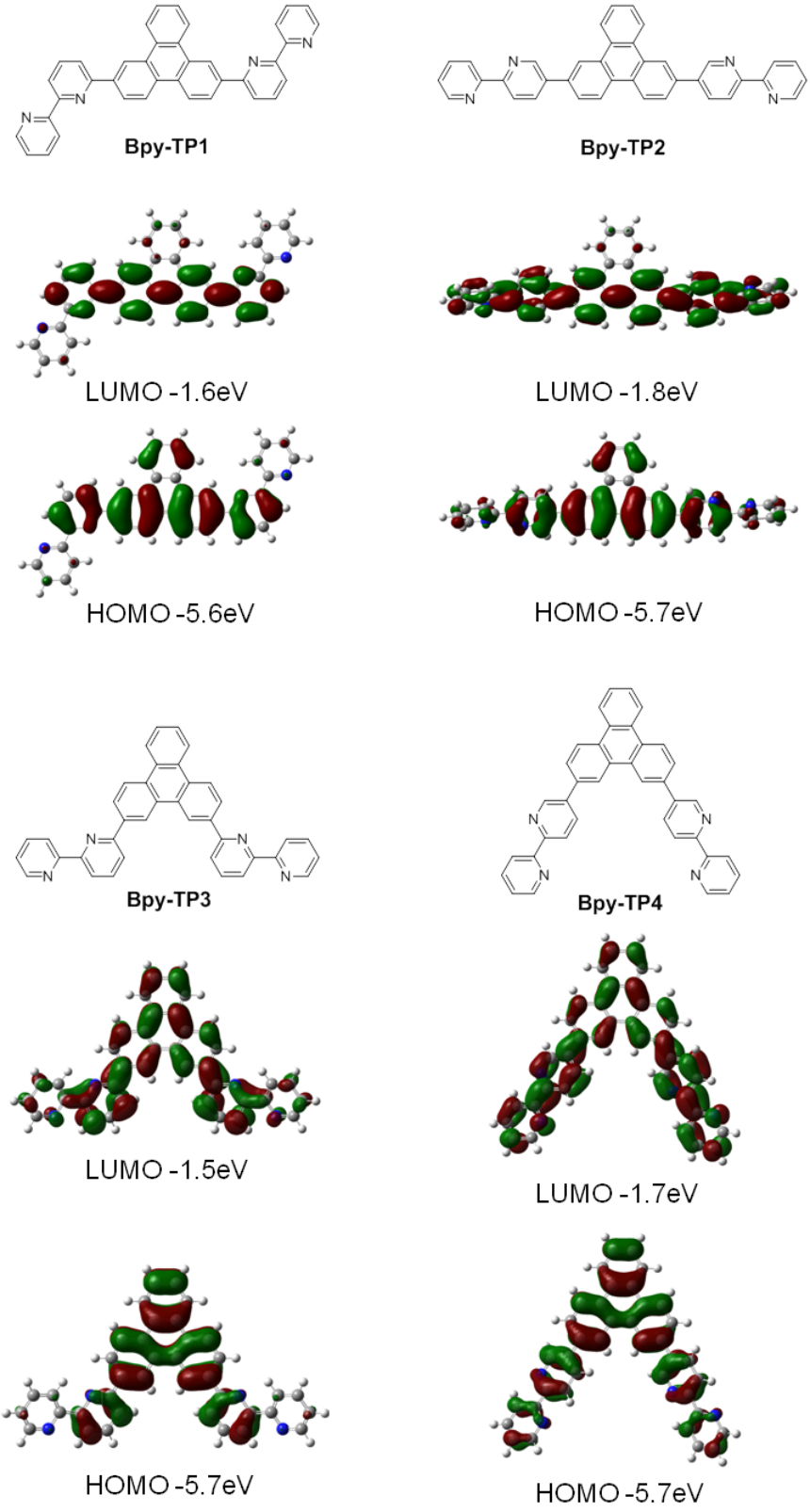

Figure 2-5. Molecular structures of Bpy-TP1, Bpy-TP2, Bpy-TP3 and Bpy-TP4 and the distributions of their HOMOs and LUMOs obtained by DFT (B3LYP/6-31G) calculations.

Figure 2-5 shows the molecular structures of Bpy-TP1, Bpy-TP2, Bpy-TP3 and Bpy-TP4 and the distributions of their LUMOs obtained by density functional theory (DFT, B3LYP/6-31G) calculations. By comparing Bpy-TP1 to Bpy-TP2, we see that the LUMO of Bpy-TP2 is widely distributed over the terminal pyridyl groups. Similarly, the LUMO of Bpy-TP4 is also distributed over the terminal pyridyl groups. The LUMO position contributes greatly to the electron injection. The electron injection efficiency can be improved by the delocalization of the LUMOs. As shown in Table 2-1, the E_a of Bpy-TP2 and Bpy-TP4 with the delocalized LUMOs are larger than those of Bpy-TP1 and Bpy-TP3.

To evaluate the electron transport properties of the triphenylene-based ETMs, green fluorescent OLEDs with a device structure of indium tin oxide (ITO, 100 nm)/4,4'-bis[*N*-(1-naphthyl)-*N*-phenylamino]biphenyl (α-NPD, 50 nm)/Alq_3 (20 nm)/ETL (30 nm)/MgAg (100 nm)/Ag (10 nm) were fabricated by vacuum deposition. Both Alq_3 and the new ETMs were tested as ETLs. First, the HTL consisting of α-NPD was deposited, followed by Alq_3 as an EML. An ETL of Alq_3 or one of the triphenylene-based materials was then deposited. Finally, MgAg and Ag layers were deposited as the cathode. The current density-voltage (*J*-*V*) characteristics of the green OLEDs with the different ETLs are shown in Fig. 2-6.

The devices with Bpy-TP1, Bpy-TP2 and Bpy-TP4 as ETLs showed lower driving voltages than that with Alq_3. As shown in Fig. 2-4, Bpy-TP1, Bpy-TP2 and Bpy-TP4 have optical anisotropy, *i.e*., they adopt a fairly parallel orientation on a substrate. In contrast, Alq_3 is known to exhibit optical isotropy, *i.e*., a completely random orientation in a deposited film.[30] It is assumed that this orientation of Bpy-TP1, Bpy-TP2 and Bpy-TP4 contributes to their improved *J*-*V* characteristics. The molecular orientation of Bpy-TP1 is higher than those

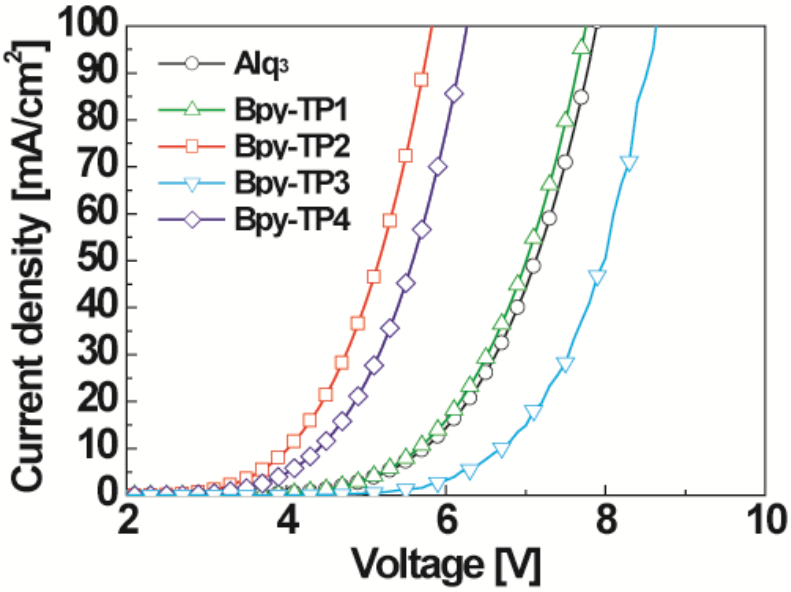

Figure 2-6. *J-V* characteristics of green fluorescent OLEDs containing different ETMs.

of Bpy-TP2 and Bpy-TP4. However, Bpy-TP1 has many possible conformers because of the rotation of the bipyridine groups, because these bipyridine groups are bonded crookedly to the central triphenylene ring. It would therefore be reasonable to assume that the overlap of the LUMOs between the molecules is disturbed, and the device with the Bpy-TP1 ETL showed a higher driving voltage compared to those with Bpy-TP2 or Bpy-TP4 ETLs. On the other hand, Bpy-TP2 and Bpy-TP4 have fewer possible conformers than Bpy-TP1 because their bipyridine groups are linearly extended to the central triphenylene ring. The device containing the Bpy-TP2 ETL showed the lowest driving voltage, while the device with the Bpy-TP3 ETL showed the highest driving voltage. We ascribe this to the lower E_a (Table 2-1) and optical isotropy (Fig. 2-4) of Bpy-TP3.

To investigate why the device with the Bpy-TP2 ETL possessed the lowest driving voltage, the dependence of the *J-V* characteristics on the film thickness was determined (Fig.

2-7 (left)). The driving voltage decreased with increasing thickness of the Bpy-TP2 layer, indicating that the high μ_e of the Bpy-TP2 layer contributes to the lower driving voltage of the OLEDs. Although the measurement of μ_e of Bpy-TP2 by the TOF method was considered, it turned out that Bpy-TP2 showed rather crystalline texture at thicker films over 1 μm, resulted in difficulty to make a thick film required for TOF measurement.

To compare the electron injection and transport properties of Alq_3, Bpy-OXDm, TPBi and Bpy-TP2, EODs containing each material as an ETL were fabricated. Figure 2-7 (right) shows the *J*-*V* characteristics of the EODs with the structure of ITO/BCP/ETL/LiF/Al.[31] Here, BCP was used as a hole blocking layer. When Bpy-TP2 was used as the ETL, electron injection was greatly improved in comparison with the devices containing Alq_3 or TPBi. While the current in the Bpy-TP2 device is lower than that with the Bpy-OXDm layer, the device containing Bpy-TP2 showed better performance at higher currents. From the slope of

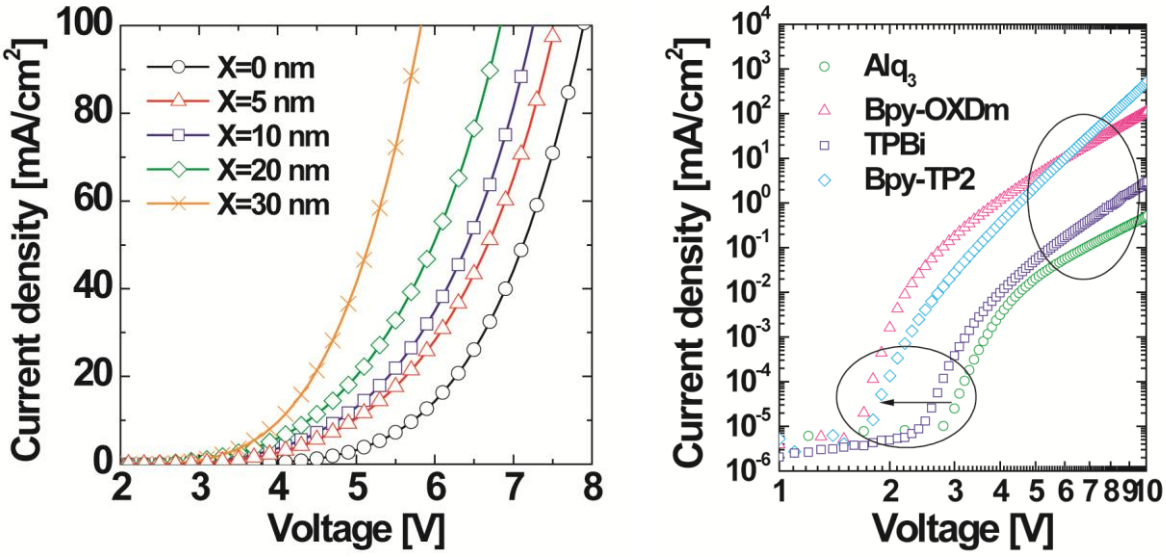

Figure 2-7. Left: Current density–voltage plots of the device structures: ITO (100 nm)/α-NPD (50 nm)/Alq_3 (50-X nm)/Bpy-TP2 (X nm)/MgAg (100 nm)/Ag (10 nm). Right: Current density–voltage plots of the EOD structures: ITO (100 nm)/BCP (10 nm)/ETL (150 nm)/LiF (1 nm)/Al (70 nm), where ETM is Alq_3, Bpy-OXDm, TPBi or Bpy-TP2.

the *J-V* curves at higher voltages, we concluded that Bpy-TP2 provides better electron transport than Alq_3, Bpy-OXDm and TPBi.

Blue fluorescent OLEDs containing Alq_3 (Device 1), TPBi (Device 2) and Bpy-TP2 (Device 3) as ETMs were also fabricated, as shown in Fig. 2-8.

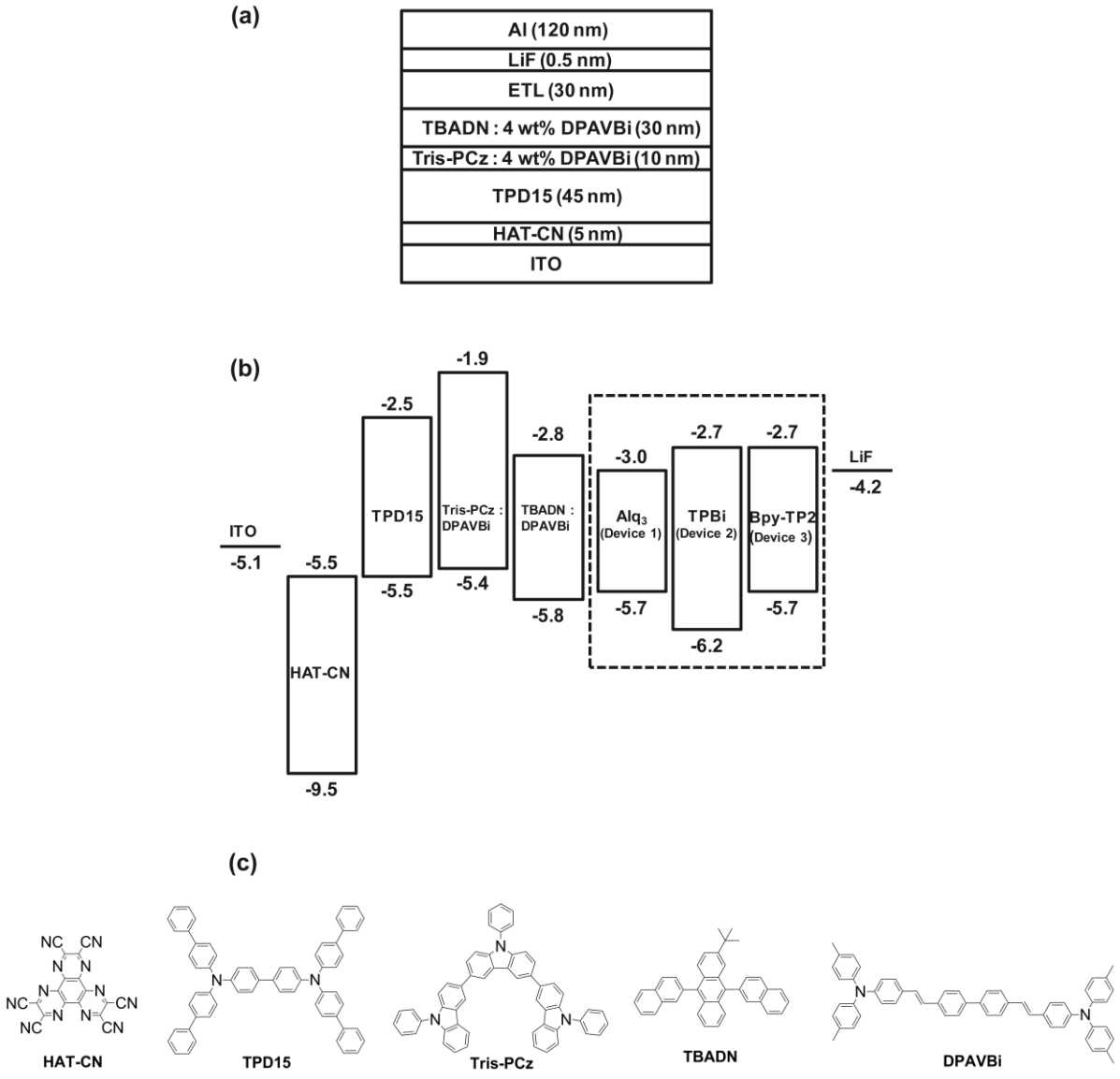

Figure 2-8. (a) Device architecture for OLEDs containing ETMs composed of Alq_3 (Device 1), TPBi (Device 2) and Bpy-TP2 (Device 3). (b) Energy diagram of the organic layers in the OLEDs. (c) Molecular structures of materials used in the OLEDs.

1,4,5,8,9,12-hexaazatriphenylene-hexacarbonitrile (HAT-CN) was used as a hole injection layer.[32] HAT-CN will promote the hole injection by using the charge separated by CT complex formed at the interface between hole injection layer (HIL) and HTL. It is suggested that charge transfer is generated from HOMO of HTM to LUMO of HAT under the condition that voltage is not impressed because HAT-CN has deeper LUMO level than conventional organic materials. The EL spectra, *J-V* characteristics and the external quantum and power efficiencies of these blue OLEDs are shown in Fig. 2-9.

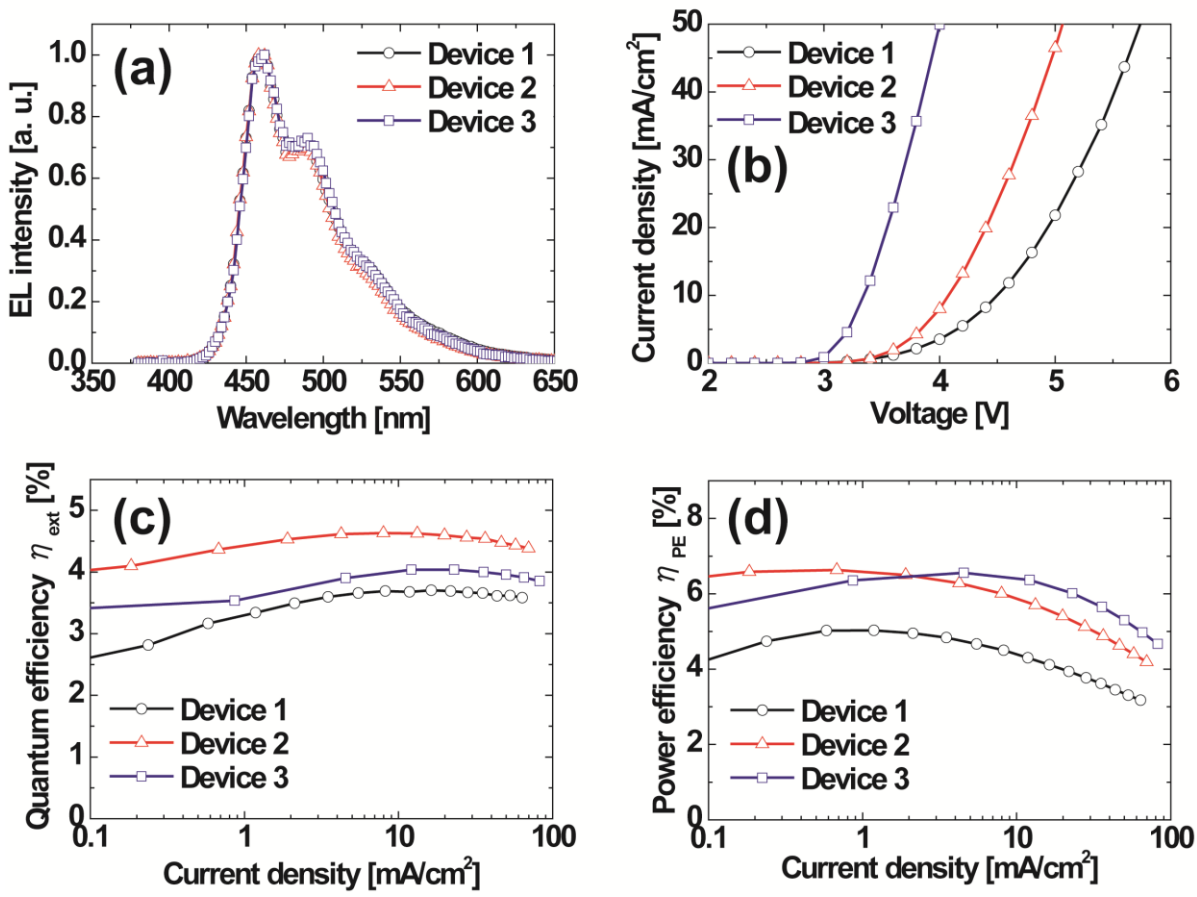

Figure 2-9. (a) EL spectra, (b) *J-V* characteristics, (c) η_{ext} against *J* and (d) η_{PE} against *J* for blue OLEDs. Details of the device architecture are shown in Fig. 2-8.

Under a constant current density of J=10 mA/cm^2, the driving voltages of Devices 1, 2 and 3 were 4.50 V, 4.07 V and 3.34 V, respectively. The driving voltage of Device 3 was dramatically reduced because of the higher μ_e and lower electron injection barrier of the Bpy-TP2 layer compared to those of the Alq_3 and TPBi layers. The external quantum efficiencies of these devices were η_{ext}=3.69%, 4.64% and 4.03% at 10 mA/cm^2, respectively. The highest η_{ext} was obtained for Device 2 because TPBi has good hole blocking properties. The power conversion efficiencies of these devices were η_{PE}=4.44%, 5.89% and 6.41% at 10 mA/cm^2, respectively. The highest η_{PE} was obtained for Device 3 at J>3 mA/cm^2.

Accelerated lifetime testing at 1000 cd/m^2 was performed for the three devices, as shown in Fig. 2-10.

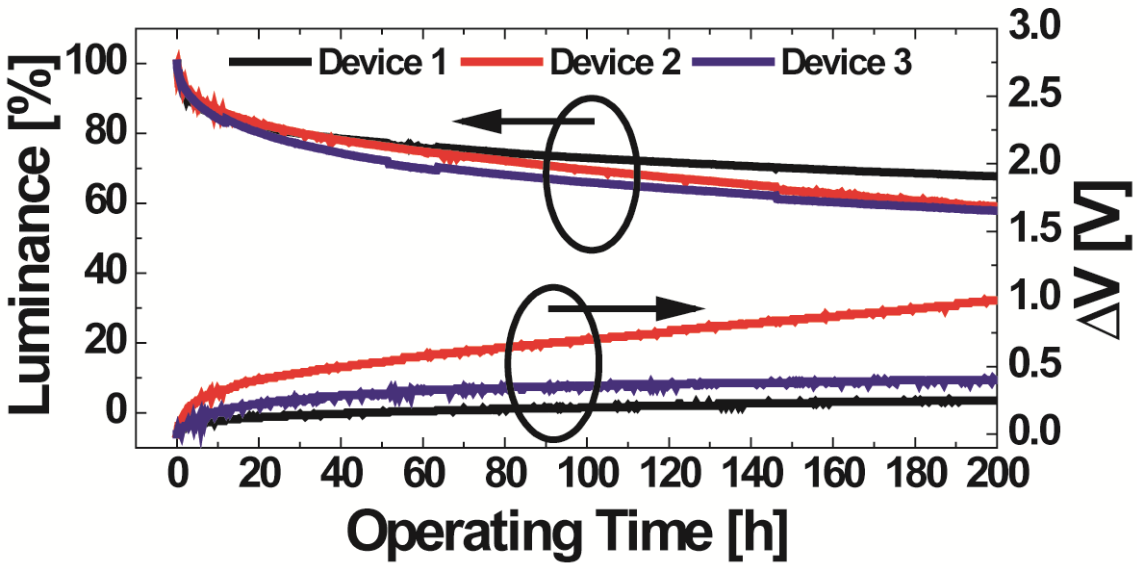

Figure 2-10. Luminance deterioration and change in driving voltage of blue OLEDs as a function of operating time at an initial luminance of 1000 cd/m^2. The device architectures are as same as those in Fig. 2-9.

The applied current and voltage were 25.2 mA/cm^2 and 4.74 V, respectively, for Device 1, 21.2 mA/cm^2 and 4.2 V, respectively, for Device 2 and 23.6 mA/cm^2 and 3.46 V, respectively, for Device 3. The preservation rates of the initial luminance for Devices 1, 2 and 3 after 200 h of continuous operation were 67.7%, 58.9% and 58.4%, respectively. The lifetime of Device 3 containing Bpy-TP2 is equivalent to that of Device 2 with TPBi. The changes in the driving voltage, ΔV, for Devices 1, 2 and 3 after 200 h were 0.25 V, 0.99 V and 0.43 V, respectively. The increased driving voltage of Device 3 was suppressed well in comparison with that of Device 2. It is believed that the larger increase in driving voltage of Device 2 was caused by degradation of the interface between the EML and ETL because of an accumulation of holes. Device 2 with TPBi can accumulate holes at the interface between the EML and the ETL more readily than the other devices because TPBi has a low HOMO level (-6.2 eV).

2-4. Conclusions

I developed triphenylene-based ETMs having optical anisotropy and good film forming properties in addition to a high E_a. In particular, the ETM having a long rod-like structure exhibited the best electron transport properties. Also, it provides improved electron transport characteristics than those of conventional ETMs such as Alq_3, Bpy-OXDm and TPBi in EODs. Furthermore, I demonstrated that new ETMs contribute to long device lifetime and suppression of an increase of driving voltage in blue OLEDs. In conclusion, the new ETMs have high potential as practical ETMs.

2-5. References

1 J. L. Bredas, S. R. Marder and E. Reichmanis, *Chem. Mater.*, **2011**, 23, 309, Thematic issue.

2 A. C. Grimsdale, K. L. Chan, R. E. Martin, P. G. Jokisz and A. B. Holmes, *Chem. Rev.*, **2009**, 109, 897.

3 C. W. Tang and S. A. VanSlyke, *Appl. Phys. Lett.*, **1987**, 51, 913.

4 C. Adachi, T. Tsutsui and S. Saito, *Appl. Phys. Lett.*, **1990**, 57, 531.

5 B. J. Chen, W. Y. Lai, Z. Q. Gao, C. S. Lee, S. T. Lee and W. A. Gambling, *Appl. Phys. Lett.*, **1999**, 75, 4010.

6 T.-Y. Chu and O.-K. Song, *Appl. Phys. Lett.*, **2007**, 90, 203512.

7 K. Tamao, M. Uchida, T. Izumizawa, K. Furukawa and S. Yamaguchi, *J. Am. Chem. Soc.*, **1996**, 118, 11974.

8 D. Tanaka, T. Takeda, T. Chiba, S. Watanabe and J. Kido, *Chem. Lett.*, **2007**, 36, 262.

9 S.-J. Su, D. Tanaka, Y.-J. Li, H. Sasabe, T. Takeda and J. Kido, *Org. Lett.*, **2008**, 10, 941.

10 M. Ichikawa, S. Fujimoto, Y. Miyazawa, T. Koyama, N. Yokoyama, T. Miki and Y. Taniguchi, *Org. Electron.*, **2008**, 9, 77.

11 R. A. Klenkler, H. Aziz, A. Tran, Z. D. Popovic and G. Xu, *Org. Electron.*, **2008**, 9, 285.

12 H.-Y. Oh, C. Lee and S. Lee, *Org. Electron.*, **2009**, 10, 163.

13 T. Matsushima, M. Takamori, Y. Miyashita, Y. Honma, T. Tanaka, H. Aihara and H. Murata, *Org. Electron.*, **2010**, 11, 16.

14 M. Ichikawa, K. Wakabayashi, S. Hayashi, N. Yokoyama, T. Koyama and Y. Taniguchi, *Org. Electron.*, **2010**, 11, 1966.

15 R. G. Kepler, P. M. Beeson, S. J. Jacobs, R.A. Anderson, M. B. Sinclair, V. S. Valencia and P. A. Cahill, *Appl. Phys. Lett.*, **1995**, 66, 3618.

16 C. Adachi, T. Tsutsui and S. Saito, *Appl. Phys. Lett.*, **1989**, 55, 1489.

17 M. Ichikawa, T. Kawaguchi, K. Kobayashi, T. Miki, K. Furukawa, T. Koyama and Y. Taniguchi, *J. Mater. Chem.*, **2006**, 16, 221.

18 D. Yokoyama, A. Sakaguchi, M. Suzuki and C. Adachi, *Appl. Phys. Lett.* **2009**, 95, 243303.

19 C. Poriel, N. Cocherel, J. Rault-Berthelot, L. Vignau and O. Jeannin, *Chem. Eur. J.*, **2011**, 17, 12631.

20 S. Tao, Y. Jiang, S.-L. Lai, M.-K. Fung, Y. Zhou, X. Zhang, W. Zao and C.-S. Lee, *Org. Electron.*, **2011**, 12, 358.

21 Y. Zhang, S.-L. Lai, Q.-X. Tong, M.-F. Lo, T.-W. Ng, M.-Y. Chan, Z.-C. Wen, J. He, K.-S. Jeff, W.-M. Liu, K. Chi-Chiu, P. Wang and C.-S. Lee, *Chem. Mater.*, **2012**, 24, 61.

22 D. Thirion, M. Romain, J. Rault-Berthelot and C. Poriel, *J. Mater. Chem.*, **2012**, 22, 7149.

23 N. Miyaura, T. Yanagi and A. Suzuki, *Synth. Commun.*, **1981**, 11, 513.

24 W.-C. Shieh and J. A. Carlson, *J. Org. Chem.*, **1992**, 57, 379.

25 B. T. King, J. Kroulik, C. R. Robertson, P. Rempala, C. L. Hilton, J. D. Korinek and L. M. Gortari, *J. Org. Chem.*, **2007**, 72, 2279.

26 T. Ishiyama, M. Murata and N. Miyaura, *J. Org. Chem.*, **1995**, 60, 7508.

27 N. Campbell and A. H. Scott, *J. Chem. Soc. C.*, **1966**, 11, 1050.

28 M. Shimizu, I. Nagao, Y. Tomioka, T. Kadowaki and T. Hiyama, *Tetrahedron.*, **2011**, 67, 8014.

29 H. Sasabe, E. Gonmori, T. Chiba, Y.-J. Li, D. Tanaka, S.-J. Su, T. Takeda, Y.-J. Pu, K. Nakayama and J. Kido, *Chem. Mater.*, **2008**, 20, 5951.

30 D. Yokoyama, A. Sakaguchi, M. Suzuki and C. Adachi, *Appl. Phys. Lett.*, **2008**, 93, 173302.

31 M. A. Khan, Wei Xu, Khizar-ul-Haq, Yu Bai, X. Y. Jiang, Z. L. Zhang and W. Q. Zhu, *J. Appl. Phys.*, **2008**, 103, 014509.

32 L. S. Liao, W. K. Slusarek, T. K. Hatwar, M. L. Ricks and D. L. Comfort, *Adv. Mater.*, **2008**, 20, 324.

Chapter 3

Molecular Design aimed for Molecular Orientation and Application as an Electron Transport Material in Organic Light-Emitting Diodes

3-1. Introduction

OLEDs have been attracting considerable attention because of their high potential for use in practical applications such as flat panel displays and lighting. Generally, the suppression of the driving voltage in OLEDs is indispensable to achieve their low-power-consumption. In order to suppress driving voltage in OLEDs, improving charge injection efficiency from an electrode and charge mobilities of charge transport layers has been required. Especially, the development of ETMs with a high μ_e is important because hole mobilities are usually much higher than μ_e in OLEDs.[1,2] To improve μ_e, strong intermolecular interaction should be required because it leads to large overlaps of π-orbitals which participate in electron transport. In particular, horizontal orientation of molecules to a substrate is an efficient way to achieve higher intermolecular interaction. Previously, Yokoyama *et al.*[3,4] have reported the horizontal orientation of molecules having long rod-like or planar structure to a substrate.

In *Chapter 2*, although I reported the molecular orientation of Bpy-TP2 (2,2′-Bpy-TP), the value of orientation parameter, S, is rather low (S=-0.1) in spite of the long rod-like molecular structure. In recent years, Yokoyama *et al.*[5] have reported that the B3 and B4PyMPM molecules having nitrogen atoms in the pyridine rings at the outer side of the molecule have larger anisotropies compared with that of the B2PyMPM in their deposited thin films because they can be connected by intermolecular C-H···N hydrogen bonds (Fig. 3-1). Using this guideline of molecular design, I designed and synthesized novel two ETMs, 2,3′-Bpy-TP and 2,4′-Bpy-TP, with the nitrogen atoms in the pyridine rings at the outer side of the 2,2′-Bpy-TP molecules.

Here, I report their molecular orientation of the deposited thin films by using VASE analysis and electron transport properties in EODs and OLEDs.

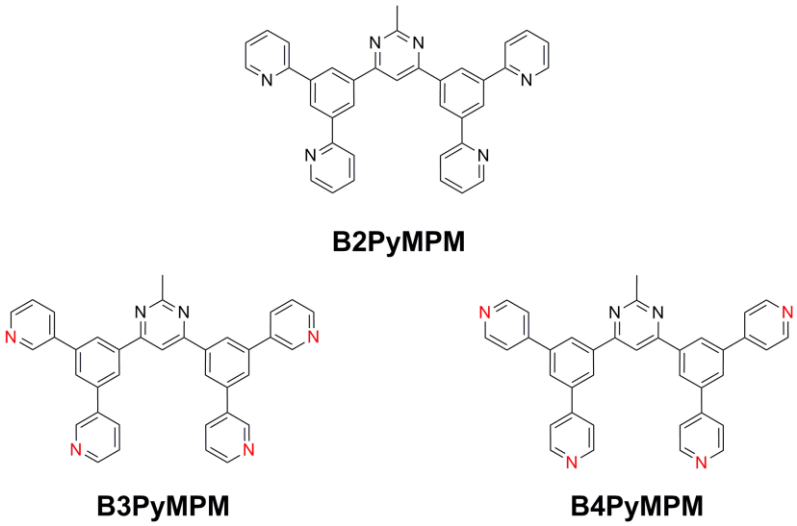

Figure 3-1. Chemical structures of B2PyMPM, B3PyMPM and B4PyMPM.

3-2. Experimental section

The chemical structures of 2,3′-Bpy-TP and 2,4′-Bpy-TP are shown in Fig. 3-2. These materials were synthesized by Suzuki-Miyaura coupling reaction[6,7] and purified by sublimation before characterization.

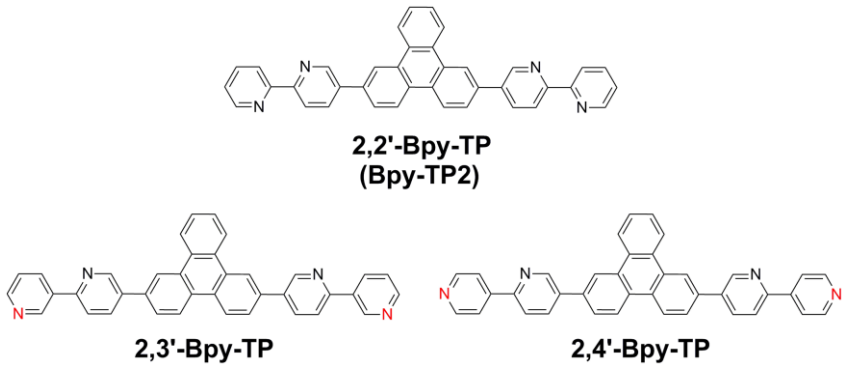

Figure 3-2. Chemical structures of 2,2′-Bpy-TP, 2,3′-Bpy-TP and 2,4′-Bpy-TP.

Synthesis

The synthetic route used to obtain 2,3′-Bpy-TP and 2,4′-Bpy-TP is outlined in Scheme 3-1.

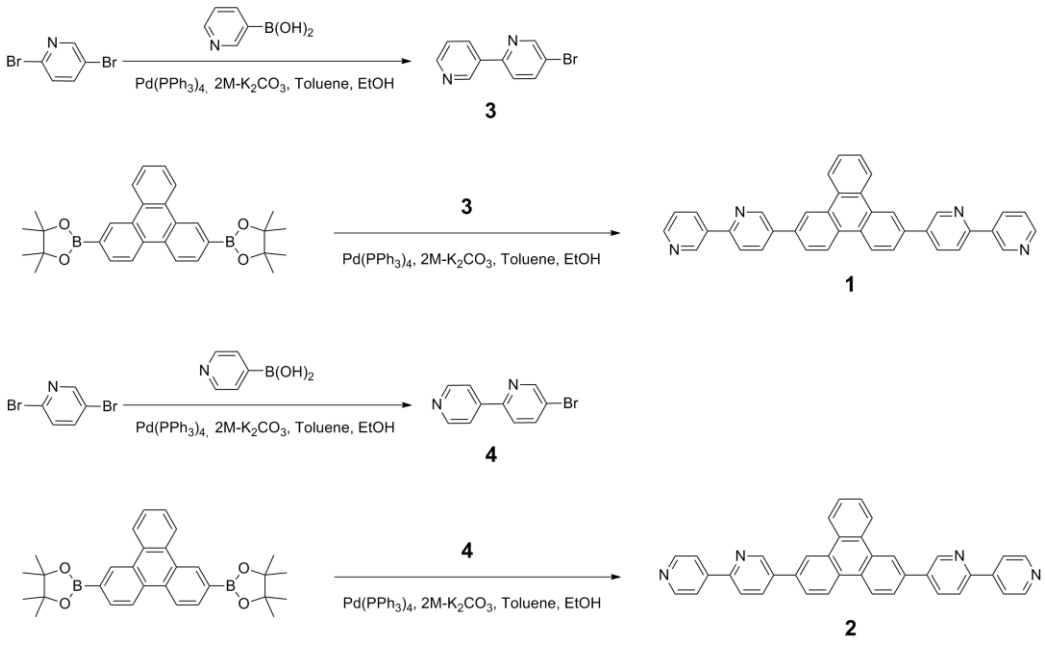

Scheme 3-1. Synthesis route for 2,3′-Bpy-TP (**1**) and 2,4′-Bpy-TP (**2**).

*(**3**) 5-bromo-2,3′-bipyridine*

A mixture of 2,5-dibromopyridine (81.4 mmol), 3-pyridineboronic acid (40.7 mmol), tetrakis(triphenylphosphine)palladium(0) (2.04 mmol), aqueous K_2CO_3 (2.0 M, 31.6 mL), toluene (100 mL), and ethanol (25 mL) was added to a flask. The mixture was degassed and heated under reflux for 6 h under an argon atmosphere. The mixture was cooled to room temperature. The crude product was extracted with toluene, dried with $MgSO_4$, filtered to remove any precipitate, and then distilled to remove solvent. Purification by column chromatography on NH silica gel with a 1/3 (=v/v) ethyl acetate/*n*-hexane mixture gave a white powder. Yield: 68%. ^{1}H NMR (500 MHz, $CDCl_3$, TMS): 7.41 (1H, m), 7.66 (1H, d, *J*=8.5 Hz), 7.92 (1H, dd, *J*=8.5 Hz), 8.30 (1H, tt, *J*=8.0 Hz), 8.67 (1H, dd, *J*=5.0), 8.77 (1H, s), 9.17 (1H, s).

*(**4**) 5-bromo-2,4′-bipyridine*

A mixture of 2,5-dibromopyridine (40.5 mmol), 4-pyridineboronic acid (20.3 mmol), tetrakis(triphenylphosphine)palladium(0) (1.3 mmol), aqueous K_2CO_3 (2.0 M, 15.2 mL), toluene (50 mL), and ethanol (40 mL) was added to a flask. The mixture was degassed and heated under reflux for 24 h under a nitrogen atmosphere. The mixture was cooled to room temperature. The crude product was extracted with chloroform, dried with $MgSO_4$, filtered to remove any precipitate, and then distilled to remove solvent. Purification by column chromatography on silica gel with a 1/1 (=v/v) toluene/ethyl acetate mixture gave a white powder. Yield: 69%. ^{1}H NMR (500 MHz, $CDCl_3$, TMS): 7.71 (1H, d, *J*=9.0 Hz), 7.87 (2H, dd, *J*=6.5 Hz), 7.95 (1H, dd, *J*=10.5 Hz), 8.74 (2H, dd, *J*=6.5 Hz), 8.80 (1H, s).

*(**1**) 2,7-Bis([2,3'-bipyridin]-5-yl)triphenylene (2,3´-Bpy-TP)*

A mixture of 2,7-bis(4,4,5,5-tetramethyl-1,3,2-dioxaborolan-2-yl)triphenylene[8] (5.6 mmol), **3** (11.8 mmol), tetrakis(triphenylphosphine)palladium(0) (0.3 mmol), aqueous K_2CO_3 (2.0 M, 8.7 mL), toluene (60 mL) and ethanol (15 mL) was mixed in a flask. The mixture was degassed and heated under reflux for 8 h under an argon atmosphere. The mixture was cooled to room temperature and then filtered. *o*-Dichlorobenzene (700 mL) was added and the mixture was stirred at 160 ºC. Then, the solution was cooled to 100 ºC and filtered to remove the precipitate. Removal of the solvent by distillation gave a crude pale yellow powder. Recrystallization from *o*-dichlorobenzene and washing with toluene/ethyl acetate yielded 2,3´-Bpy-TP as a pale yellow powder. Yield: 61%. Mp: 362 ºC. UV/Vis (film): λ_{max}=367 nm. ^{1}H NMR (400 MHz, DMSO d-6): 7.53 (2H, m), 7.78 (2H, m), 8.15 (4H, m), 8.49 (4H, m), 8.65 (2H, dd, *J*=4.8 Hz), 8.94 (2H, d, *J*=8.4 Hz), 9.02 (2H, m), 9.14 (2H, s), 9.31 (2H, s), 9.34 (2H, s). Elemental analysis: Found C, 85.11%; H, 4.44%; N, 10.38%; Calc. for $C_{38}H_{24}N_4$: C, 85.05%, H, 4.51%; N, 10.44%; MS (MALDI-TOF): *m*/*z* 537.17 $[M]^{+\cdot}$.

*(**2**) 2,7-Bis([2,4'-bipyridin]-5-yl)triphenylene (2,4´-Bpy-TP)*

A mixture of 2,7-bis(4,4,5,5-tetramethyl-1,3,2-dioxaborolan-2-yl)triphenylene (4.2 mmol), **4** (10.2 mmol), tetrakis(triphenylphosphine)palladium(0) (0.3 mmol), aqueous K_2CO_3 (2.0 M, 6.3 mL), toluene (40 mL) and ethanol (25 mL) was mixed in a flask. The mixture was degassed and heated under reflux for 24 h under a nitrogen atmosphere. The mixture was cooled to room temperature and then filtered. *o*-Dichlorobenzene (1300 mL) was added and the mixture was stirred at 160 ºC. Then, the solution was cooled to 100 ºC and filtered to remove the precipitate. Removal of the solvent by distillation gave a crude pale yellow

powder. Recrystallization from *o*-dichlorobenzene yielded 2,4´-Bpy-TP as a pale yellow powder. Yield: 52%. Mp: 423 ºC. UV/Vis (film): λ_{max}=357 nm. Elemental analysis: Found C, 85.08%; H, 4.42%; N, 10.39%; Calc. for $C_{38}H_{24}N_4$: C, 85.05%, H, 4.51%; N, 10.44%; MS (MALDI-TOF): *m*/*z* 537.16 $[M]^{+\cdot}$.

3-3. Results and discussion

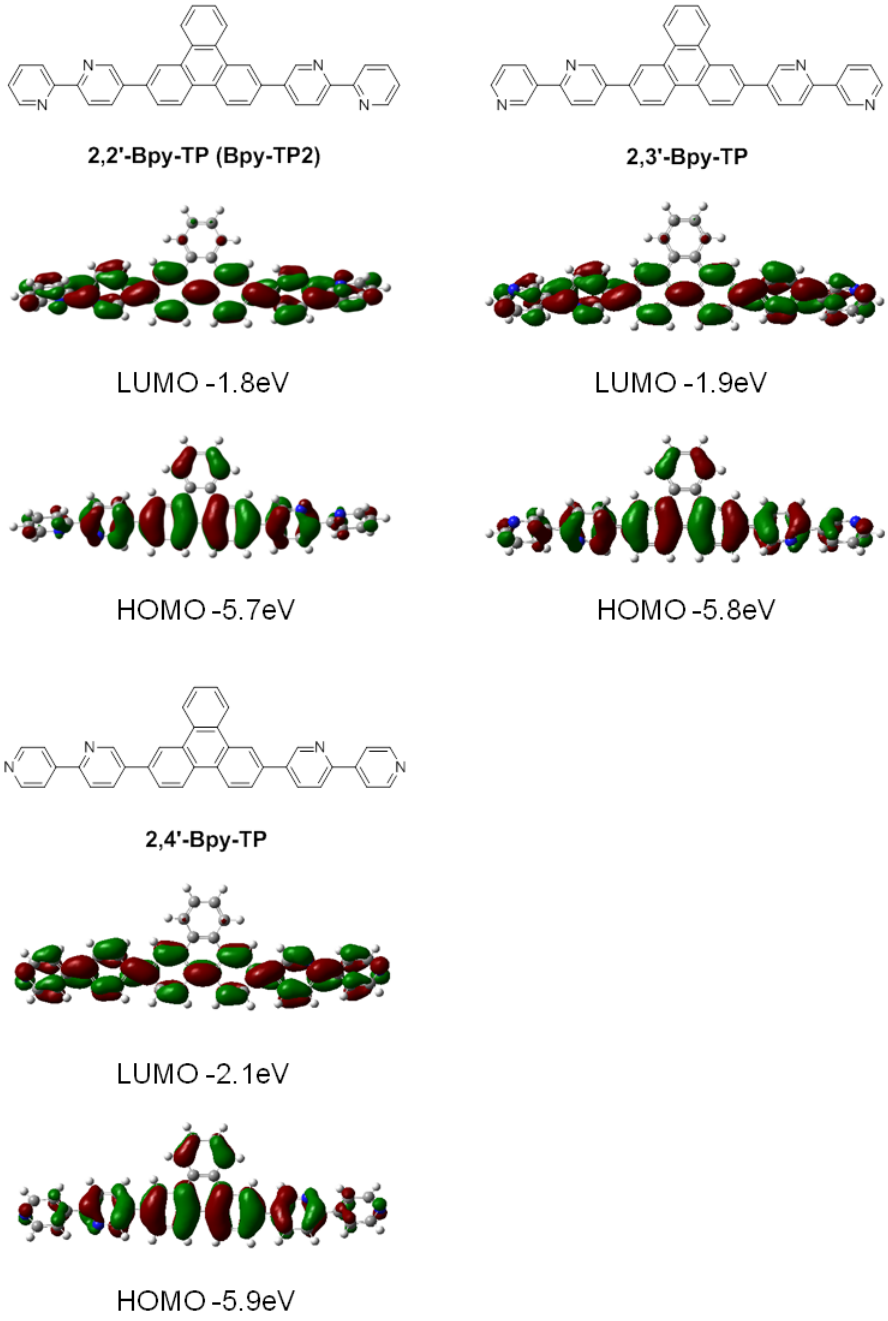

Figure 3-3. Molecular structures of 2,2′-Bpy-TP (Bpy-TP2), 2,3′-Bpy-TP and 2,4′-Bpy-TP and the distributions of their HOMOs and LUMOs obtained by DFT (B3LYP/6-31G) calculations.

Figure 3-3 shows molecular structures of 2,2′-Bpy-TP, 2,3′-Bpy-TP and 2,4′-Bpy-TP and the distributions of LUMOs obtained by DFT (B3LYP/6-31G) calculations. Their

LUMOs are similarly distributed over the terminal pyridyl groups. The LUMO values of 2,3′-Bpy-TP and 2,4′-Bpy-TP obtained by DFT calculations are relatively deeper than that of 2,2′-Bpy-TP.

The crude ETMs were sublimed, and their thermophysical properties were measured by DSC. Their optical and photophysical properties were also evaluated by AC-3, UV-vis absorption and PL spectroscopies. Figure 3-4 shows UV-vis absorption and PL spectra of 2,3′-Bpy-TP and 2,4′-Bpy-TP in dichloromethane solution and neat films. The molecular orientation of their deposited thin films was evaluated by VASE measurements. The physical properties of 2,2′-Bpy-TP, 2,3′-Bpy-TP and 2,4′-Bpy-TP are summarized in Table 3-1.[9]

As shown in Table 3-1, 2,3′-Bpy-TP and 2,4′-Bpy-TP have a low-lying HOMO level compared to 2,2′-Bpy-TP, indicating that they exhibit higher hole blocking properties than 2,2′-Bpy-TP when used as ETL in OLEDs. The LUMO values of 2,3′-Bpy-TP and 2,4′-Bpy-TP estimated from the difference between I_p and E_g are also much deeper than that of 2,2′-Bpy-TP similar to the LUMO values obtained by DFT calculations, indicating that they exhibit improved electron injection properties from a cathode than that of 2,2′-Bpy-TP.

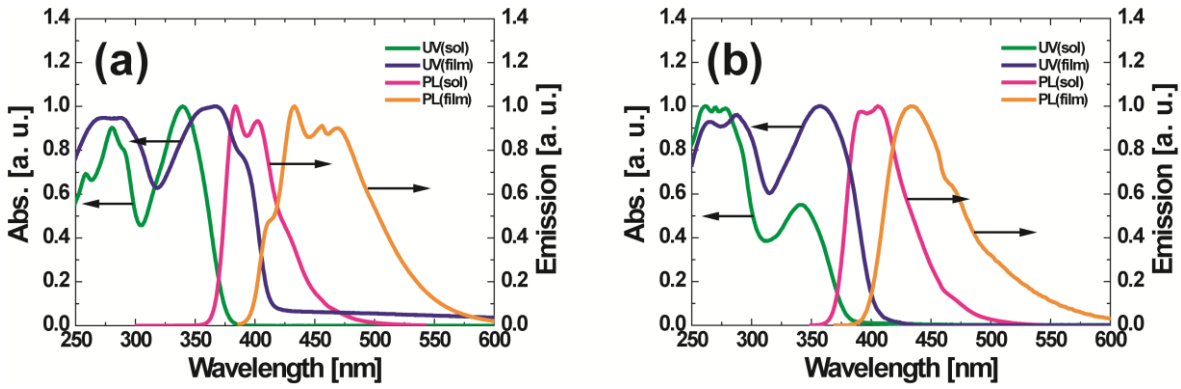

Figure 3-4. UV-vis absorption and PL spectra of (a) 2,3′-Bpy-TP and (b) 2,4′-Bpy-TP in dichloromethane solution and neat films.

Table 3-1. Physical properties of triphenylene-based ETMs

	T_m [a] (°C)	T_g [b] (°C)	E_g [c] (eV)	I_p [d] (eV)	I_p [e] (eV)	E_a [f] (eV)	E_a [g] (eV)
2,2'-Bpy-TP	338	N.O.	3.0	-5.7	-5.7	-1.8	-2.7
2,3'-Bpy-TP	362	N.O.	3.0	-5.8	-6.2	-1.9	-3.2
2,4'-Bpy-TP	423	−	3.0	-5.9	-6.2	-2.1	-3.2

[a] Melting point. [b] Glass transition temperature. [c] Energy gap estimated from the absorption edge of the films. [d] Ionization potential obtained by DFT (B3LYP/6-31G) calculation. [e] Ionization potential determined by AC-3 measurements. [f] Eelectron affinity obtained by DFT (B3LYP/6-31G) calculation. [g] Electron affinity estimated from the difference between I_p [e] and E_g [c].

The molecular orientation of their deposited thin films was investigated using VASE analysis along with *Chapter 2*. I can quantify the molecular orientation in an amorphous film using the orientation parameter S.[3] As shown in Fig. 3-5, the values of S determined from VASE analysis are S=-0.4 for 2,3′-Bpy-TP and S=-0.3 for 2,4′-Bpy-TP. The deposited thin films of 2,3′-Bpy-TP and 2,4′-Bpy-TP possess much larger optical anisotropy than that of 2,2′-Bpy-TP, indicating that their molecules in an amorphous thin film tend to almost orient horizontally to a substrate. I demonstrated that the substitution of end groups greatly affected horizontal orientation of molecules having a rod-like structure.

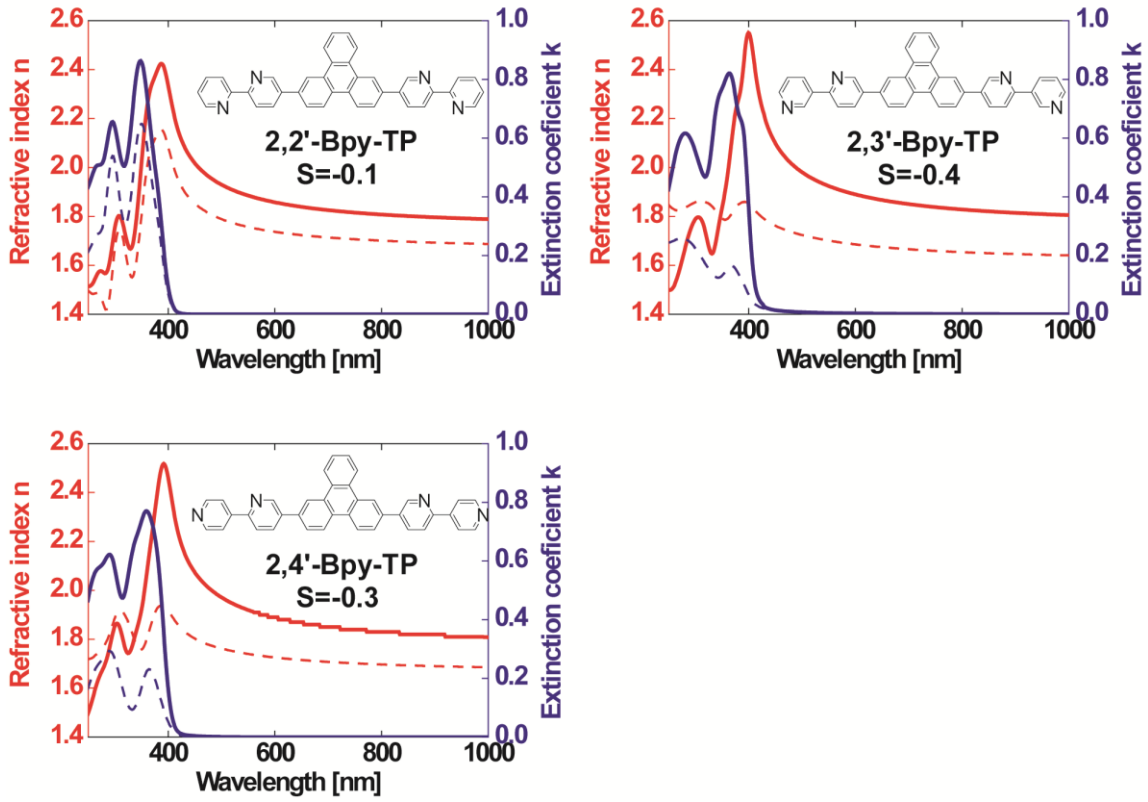

Figure 3-5. Refractive indices (red) and extinction coefficients (blue) of synthesized ETMs. The solid and broken lines indicate the ordinary and extraordinary components of the optical constants, respectively.

To compare the electron transport properties of Alq_3, 2,2′-Bpy-TP, 2,3′-Bpy-TP and 2,4′-Bpy-TP, the EODs containing each ETM were fabricated. Figure 3-6 (Left) shows the *J-V* characteristics of the EODs with the structure of ITO (100 nm)/BCP (10 nm)/ETL (150 nm)/MgAg (100 nm)/Ag (10 nm).[10] Here, BCP was used as a hole blocking layer. The EODs containing 2,2′-Bpy-TP, 2,3′-Bpy-TP and 2,4′-Bpy-TP exhibited much lower driving voltage than the EOD containing Alq_3. Especially, the EOD containing 2,3′-Bpy-TP exhibited the lowest driving voltage compared with those with Alq_3, 2,2′-Bpy-TP and 2,4′-Bpy-TP. Figure 3-6 (Right) shows the relationship between driving voltage (at 1 mA/cm^2) and orientation

parameter S of ETMs. The driving voltage decreased with increasing the degree of horizontal orientation of the molecules. It could be reasonable that the μ_e of 2,3′-Bpy-TP and 2,4′-Bpy-TP have been significantly improved by the improved horizontal orientation of their molecules.

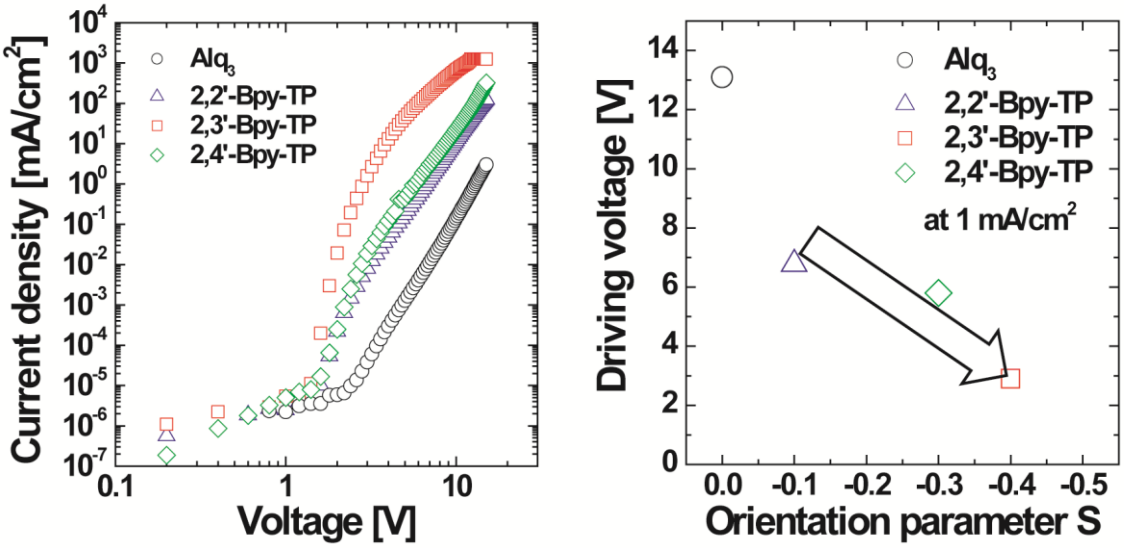

Figure 3-6. Left: *J-V* characteristics of EOD structures: ITO (100 nm)/BCP (10 nm)/ETL (150 nm)/MgAg (100 nm)/Ag (10 nm), where ETM is Alq_3, 2,2′-Bpy-TP, 2,3′-Bpy-TP and 2,4′-Bpy-TP. Right: Driving voltage–orientation parameter S of ETMs plots.

To evaluate the electron transport properties in OLEDs, green fluorescent OLEDs with a device structure of ITO (100 nm)/α-NPD (50 nm)/Alq_3 (20 nm)/ETL (30 nm)/MgAg (100 nm)/Ag (10 nm) were fabricated and evaluated. The EL spectra, *J-V* characteristics and η_{ext} of the green OLEDs with the different ETLs are shown in Fig. 3-7.

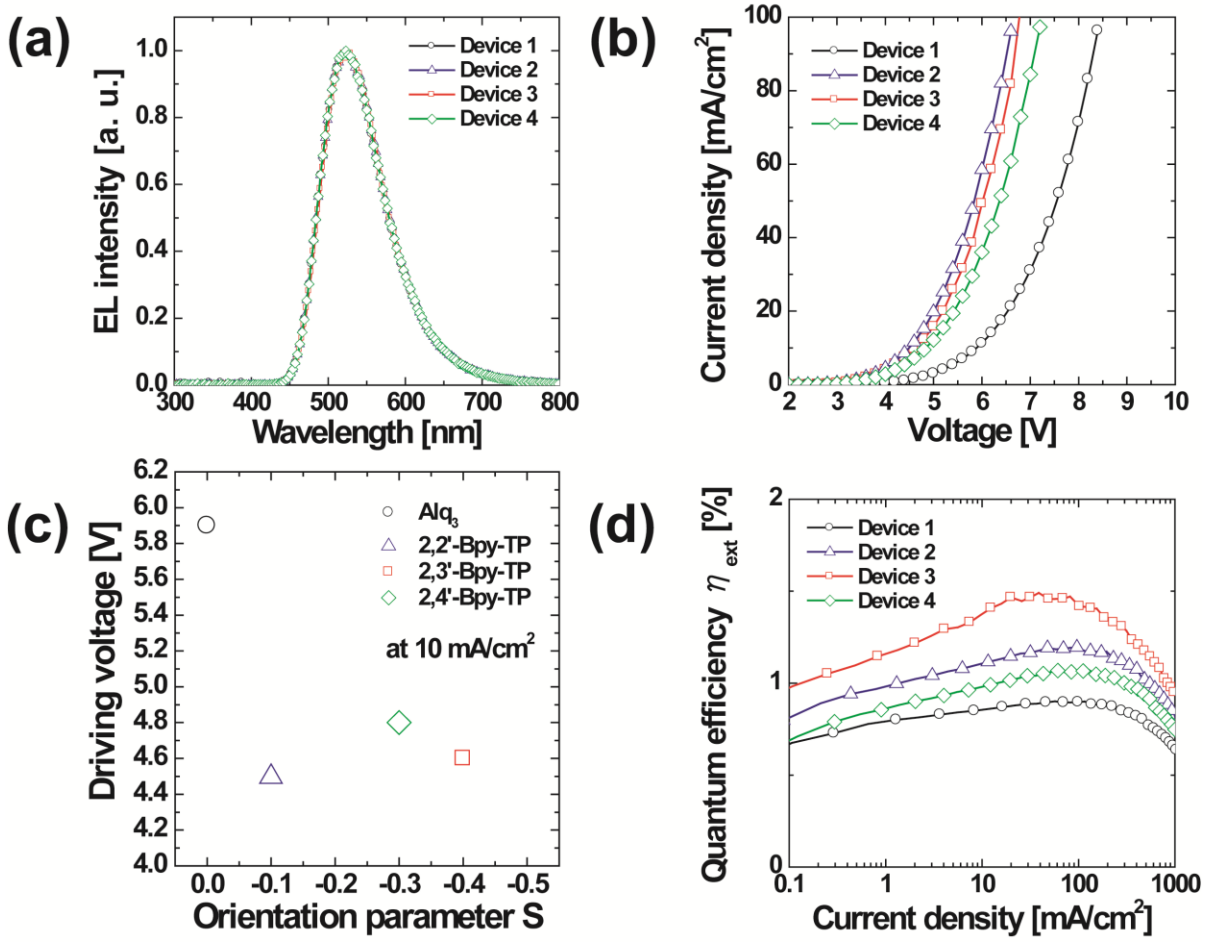

Figure 3-7. (a) EL spectra, (b) *J*-*V* characteristics, (c) Driving voltage–orientation parameter S of ETMs plots and (d) η_{ext} against *J* for the OLED structures: ITO (100 nm)/α-NPD (50 nm)/Alq_3 (20 nm)/ETL (30 nm)/MgAg (100 nm)/Ag (10 nm), where ETM is Alq_3 (Device 1), 2,2′-Bpy-TP (Device 2), 2,3′-Bpy-TP (Device 3) and 2,4′-Bpy-TP (Device 4).

All devices exhibited similar EL spectra (Fig. 3-7 (a)). Under a constant current density of J=10 mA/cm^2, the driving voltages of Devices 1, 2, 3 and 4 were 5.9, 4.5, 4.6 and 4.8 V, respectively (Fig. 3-7 (b)). Figure 3-7 (c) shows the relationship between driving voltage (at 10 mA/cm^2) and orientation parameter S of ETMs. The driving voltage decreased without depending on a value of S. Therefore, it is suggested that factors other than the horizontal

orientation of ETM contribute greatly to the improvement of the *J-V* characteristics in OLEDs. Especially, it is inferred that electron injection from ETL to EML is an important factor. In Device 2 containing 2,2′-Bpy-TP, the electron injection barrier from ETL to EML is almost zero. On the other hand, Devices 3 and 4 containing 2,3′-Bpy-TP and 2,4′-Bpy-TP, respectively, have electron injection barrier from ETL to EML because 2,3′-Bpy-TP and 2,4′-Bpy-TP possess a lower-lying LUMO level than those of Alq_3 and 2,2′-Bpy-TP (Table 3-1). Thus, it is reasonable that electron injection barrier from ETL to EML caused higher driving voltage in Devices 3 and 4 than that in Device 2 (Fig. 3-8). Here, I assume that electron injection efficiency from a cathode layer into the ETLs is almost independent on the energy barrier because the turn on voltages of EODs having 2,2′-Bpy-TP, 2,3′-Bpy-TP and 2,4′-Bpy-TP as an ETL are almost same voltage of 1.4 V (Fig. 3-6 (Left)). Therefore, in order to pull out the high electron transport properties of 2,3′-Bpy-TP and 2,4′-Bpy-TP, combining them with the EML having a lower-lying LUMO can be efficient. Further, I note η_{ext} depending on ETMs. The η_{ext} of Devices 1, 2, 3 and 4 were 0.9, 1.1, 1.4 and 1.0%, respectively, at 10 mA/cm^2 (Fig. 3-7 (d)). Therefore, there is no relationship between the molecular orientation and η_{ext}. Device 3 with 2,3′-Bpy-TP as an ETL exhibited the highest η_{ext}. This is due to the improved carrier balance in the EML caused by better electron transport in 2,3′-Bpy-TP (Fig. 3-6 (Left)). From the *J-V* characteristics and η_{ext} of OLEDs, it is inferred that the distribution of voltage which participates in injection and transport of hole and electron by recombination in an EML may be different.

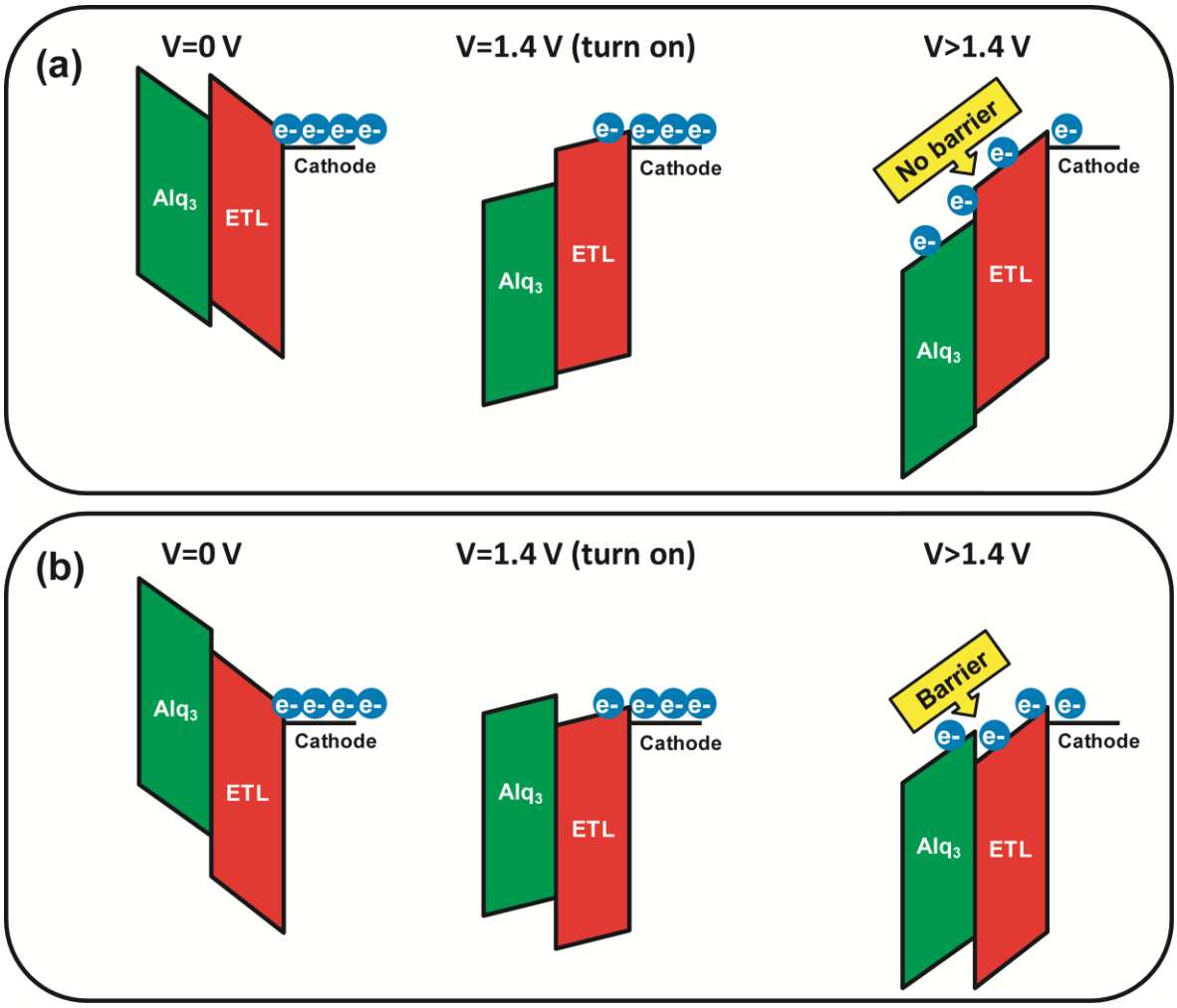

Figure 3-8. Energy diagram of EML and ETL in (a) Device 2 and (b) Devices 3 and 4. Details of the device architecture are shown in Fig. 3-7.

3-4. Conclusions

I developed high performance ETMs having a high horizontal molecular orientation and electron transport properties as shown below. Further, I demonstrated that there is closed relationship between their molecular orientation and the driving voltage of EODs containing them as an ETL. On the other hand, there is no clear relationship between their molecular orientation and the driving voltage of OLEDs containing them as an ETL since the electron injection barrier from ETL into EML significantly affects the driving voltage of OLEDs.

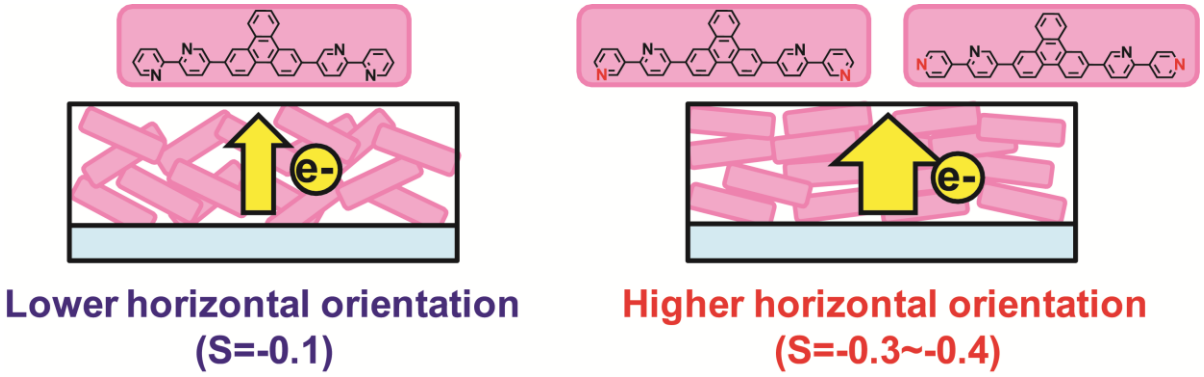

Finally, I look to the future development of ETMs. In *Chapters 2* and *3*, a planar structure of triphenylene was used for the molecular design of ETMs aiming for induction of horizontal molecular orientation. It is inferred that further expansion of molecular length should lead to the improvements of a horizontal molecular orientation and electron transport properties (Fig. 3-9 (Left)). Also, the expanding of planarity of molecular structures such as linking of bipyridyl groups should be efficient to improve a horizontal molecular orientation (Fig. 3-9 (Right)). However, we have to be careful about thin film morphologies of molecules because further extending of molecular length would lead to the high crystallinity of the deposited films.

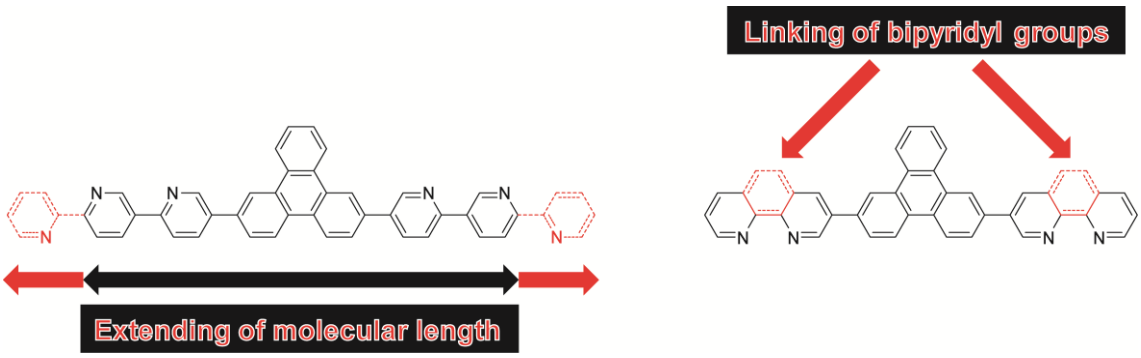

Figure 3-9. Molecular design images of ETMs aiming for induction of further horizontal molecular orientation.

3-5. References

1 B. J. Chen, W. Y. Lai, Z. Q. Gao, C. S. Lee, S. T. Lee and W. A. Gambling, *Appl. Phys. Lett.*, **1999**, 75, 4010.

2 T.-Y. Chu and O.-K. Song, *Appl. Phys. Lett.*, **2007**, 90, 203512.

3 D. Yokoyama, A. Sakaguchi, M. Suzuki and C. Adachi, *Appl. Phys. Lett.*, **2008**, 93, 173302.

4 D. Yokoyama, Y. Setoguchi, A. Sakaguchi, M. Suzuki and C. Adachi, *Adv. Funct. Mater.*, **2010**, 20, 386.

5 D. Yokoyama, H. Sasabe, Y. Furukawa, C. Adachi and J. Kido, *Adv. Funct. Mater.*, **2011**, 21, 1375.

6 N. Miyaura, T. Yanagi and A. Suzuki, *Synth. Commun.*, **1981**, 11, 513.

7 W.-C. Shieh and J. A. Carlson, *J. Org. Chem.*, **1992**, 57, 379.

8 K. Togashi, S. Nomura, N. Yokoyama, T. Yasuda and C. Adachi, *J. Mater. Chem.*, **2012**, 22, 20689.

9 H. Sasabe, E. Gonmori, T. Chiba, Y.-J. Li, D. Tanaka, S.-J. Su, T. Takeda, Y.-J. Pu, K. Nakayama and J. Kido, *Chem. Mater.*, **2008**, 20, 5951.

10 M. A. Khan, Wei Xu, Khizar-ul-Haq, Yu Bai, X. Y. Jiang, Z. L. Zhang and W. Q. Zhu, *J. Appl. Phys.*, **2008**, 103, 014509.

Chapter 4

Triphenylene-Based Host Materials for Low-Voltage and Highly Efficient Red Phosphorescent Organic Light-Emitting Diodes

4-1. Introduction

OLEDs are attracting considerable attention because of their great potential for practical application in flat panel displays and lighting. Recently, PHOLEDs have been intensively investigated to realize high luminance efficiency because their internal quantum efficiency η_{int} can reach ≈100%, corresponding to an external quantum efficiency η_{ext} of about 20%. In contrast, η_{int} is limited to 25% in fluorescent OLEDs, corresponding to η_{ext} of ≈5%.[1] However, efficiency roll-off at high current density caused by triplet-triplet annihilation (TTA) of excitons is significant in PHOLEDs.[2-4] Improving the carrier balance in the EML and broadening the carrier recombination zone can suppress such efficiency roll-off at high current density.[5,6] Recently, bipolar PH host materials containing hole-transporting (donor) and electron-transporting (acceptor) moieties have been developed to improve the carrier balance in the EML.[7-9] PHOLEDs with double-emission layers have also been developed to broaden the carrier recombination zone.[5]

To optimize device performance, PH host materials need to possess a higher E_T than that of guest emitters to confine triplet excitons in the EML. Furthermore, host layers should have balanced carrier transport properties with appropriate HOMO and LUMO levels. Finally, EMLs should have high T_g, and show good thermal stability. Conventional PH host materials CBP and mCP have rather low T_g (<100 °C) and their thin films can easily crystallize,[10-12] which reduce device lifetime.

Here, I report novel red PH host materials based on a triphenylene frame, BDBF-TP and BDBT-TP (Fig. 4-1), that possess high T_g and good carrier transport properties. These novel PH host materials are useful for low voltage, highly efficient red PHOLEDs.

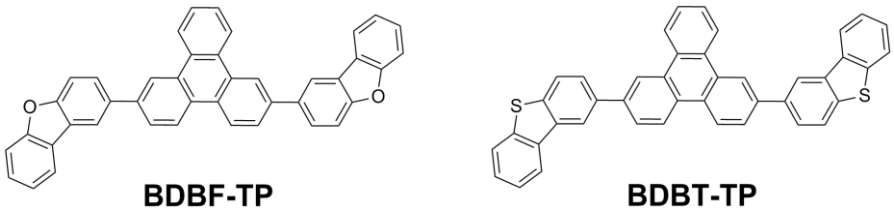

Figure 4-1. Chemical structures of BDBF-TP and BDBT-TP.

4-2. Experimental section

The chemical structures of BDBF-TP and BDBT-TP are shown in Fig. 4-1. The materials were synthesized by the Suzuki-Miyaura coupling reaction[13,14] and then purified by sublimation before characterization.

Synthesis

The synthesis route used to obtain BDBF-TP and BDBT-TP is outlined in Scheme 4-1. 2-Bromodibenzofuran[15] was prepared according to previously reported procedures.

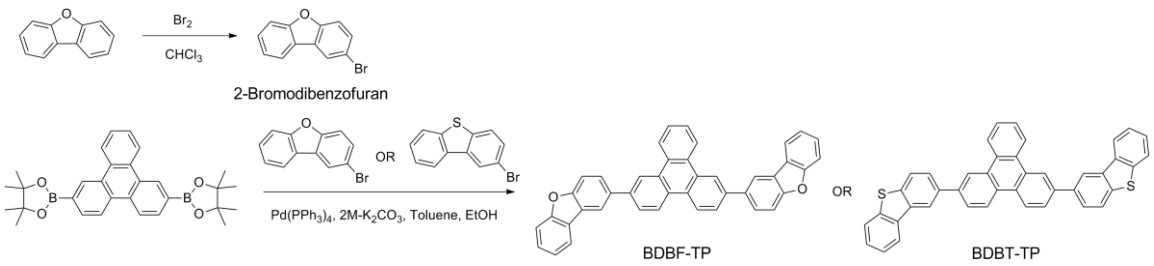

Scheme 4-1. Synthesis route for BDBF-TP and BDBT-TP.

2-Bromodibenzofuran

A mixture of dibenzofuran (59.5 mmol), bromine (53.6 mmol), and acetic acid (60 mL) was added to a flask. The mixture was stirred at room temperature for 24 h and filtered. Purification by washing with methanol produced a white powder. Yield: 23%. ^{1}H NMR (500 MHz, $CDCl_3$, TMS): δ (ppm) 7.36 (1H, t, *J*=7.5 Hz), 7.44 (1H, d, *J*=8.5 Hz), 7.48 (1H, t, *J*=8.5 Hz), 7.55 (2H, m), 7.91 (1H, d, *J*=8.0 Hz), 8.07 (1H, s).

2,7-Bis(dibenzofuran-2-yl)triphenylene (BDBF-TP)

A mixture of 2,7-Bis(4,4,5,5-tetramethyl-1,3,2-dioxaborolan-2-yl)triphenylene[16] (5.2 mmol), 2-Bromodibenzofuran (11.4 mmol), tetrakis(triphenylphosphine)palladium(0) (0.26 mmol), aqueous K_2CO_3 (2.0 M, 8.0 mL), toluene (60 mL) and ethanol (15 mL) was added to a flask. The mixture was degassed and then heated under reflux for 7 h under an argon atmosphere. The mixture was then cooled to room temperature and filtered. THF (150 mL) was added, and the solid was dissolved at 65 °C. The solution was cooled to 40 °C and then filtered to remove the Pd catalyst. The solvent was removed by distillation to leave a crude off-white powder. Recrystallization from *o*-dichlorobenzene, washing with toluene and washing with methanol yielded BDBF-TP as an off-white powder. Yield: 57%. Mp: 287 °C. UV/Vis (THF): λ_{max}=322 nm. ^{1}H NMR (400 MHz, DMSO d-6): δ (ppm) 7.45 (2H, t, *J*=7.0 Hz), 7.56 (2H, t, *J*=7.3 Hz), 7.71 (2H, d, *J*=7.7 Hz), 7.81 (4H, m), 8.11 (4H, m), 8.29 (2H, d, *J*=7.3 Hz), 8.71 (2H, s), 8.91 (2H, d, *J*=8.4 Hz), 9.03 (2H, s), 9.11 (2H, s). Elemental analysis: found C, 90.11%; H, 4.21%; calc. for $C_{42}H_{24}O_2$: C, 89.98%, H, 4.31%, O, 5.71%; MS (MALDI-TOF): *m*/*z* 560.31 $[M]^{+\cdot}$.

2,7-Bis(dibenzothiophen-2-yl)triphenylene (BDBT-TP)

A mixture of 2,7-Bis(4,4,5,5-tetramethyl-1,3,2-dioxaborolan-2-yl)triphenylene (5.2 mmol), 2-Bromodibenzothiophene (11.5 mmol), tetrakis(triphenylphosphine)palladium(0) (0.26 mmol), aqueous K_2CO_3 (2.0 M, 8.0 mL), toluene (60 mL) and ethanol (15 mL) was mixed in a flask. The mixture was degassed and then heated under reflux for 8 h under an argon atmosphere. The mixture was cooled to room temperature and then filtered. THF (200 mL) was added to the mixture and then stirred at 50 °C. The solution was then cooled to room temperature and filtered to remove the Pd catalyst. The solvent was removed by distillation to leave a crude pale yellow powder. Recrystallization from *o*-dichlorobenzene and washing

with toluene/ethyl acetate yielded BDBT-TP as an off-white powder. Yield: 58%. Mp: 300 °C. UV/Vis (THF): λ_{max}=333 nm. ^{1}H NMR (400 MHz, DMSO d-6): δ (ppm) 7.56 (4H, t, 3.7 Hz), 7.80 (2H, m), 8.03 (2H, m), 8.11 (2H, d, *J*=8.4 Hz), 8.16 (2H, d, *J*=8.4 Hz), 8.21 (2H, d, *J*=8.8 Hz), 8.61 (2H, m), 8.94 (4H, m), 9.07 (2H, m), 9.18 (2H, s). Elemental analysis: found C, 84.97%; H, 3.99%; calc. for $C_{42}H_{24}S_2$: C, 85.10%, H, 4.08%, S, 10.82%; MS (MALDI-TOF): *m*/*z* 592.14 $[M]^{+\cdot}$.

4-3. Results and discussion

The novel PH host materials were designed to achieve high carrier transport properties and E_T. Although triphenylene is a planar condensed polycyclic aromatic unit, it has a high E_T (2.9 eV). Dibenzofuran and dibenzothiophene also exhibit high E_T (3.0 eV). In addition, triphenylene has been used as a core unit in liquid crystals which shows high carrier mobilities.[17] Therefore, two dibenzofuran or dibenzothiophene units were attached at the 2 and 7 positions of a triphenylene core. The crude PH host materials were sublimed and their thermophysical properties were measured by DSC. Their optical and photophysical properties were evaluated by a Riken AC-3, UV-Vis absorption and PL spectroscopies. The thermophysical and optical properties of BDBF-TP and BDBT-TP are summarized in Table 4-1.[18]

Table 4-1. Physical properties of triphenylene-based red PH host materials.

	T_m[a] (°C)	T_g[b] (°C)	E_g[c] (eV)	HOMO[d] (eV)	LUMO[e] (eV)	λ_{abs}[f] (nm)	λ_{PL} (nm)	Φ_{PL}[g] (%)	E_T (eV)
BDBF-TP	285	106	3.2	-6.0	-2.8	334	412	62	2.51
BDBT-TP	300	125	3.1	-6.0	-2.9	341	430	45	2.49

[a] Melting point. [b] Glass transition temperature. [c] Energy gap estimated from the absorption edge of the films. [d] Determined by AC-3 measurements. [e] LUMO=HOMO+E_g. [f] Only the lowest energy absorption maxima are given. [g] Absolute PL quantum yield measured using an integrating sphere.

Figure 4-2 shows the UV-Vis absorption and PL spectra of BDBF-TP and BDBT-TP in solution (THF) and solid thin films. The T_g are 106 °C for BDBF-TP and 125 °C for BDBT-TP, which are higher than those of conventional PH host materials CBP and mCP, indicating that BDBF-TP and BDBT-TP have excellent thermal and morphological stabilities.

The LUMO levels for BDBF-TP (-2.8eV) and BDBT-TP (-2.9eV) were estimated from their HOMO levels and E_g, and indicate that they have higher E_a than CBP and mCP. Phosphorescence (Phos) spectra of BDBF-TP and BDBT-TP in THF at 77 K show the highest-energy emission maxima at 495 and 497 nm, respectively, corresponding to E_T of ≈2.5 eV. The E_T is higher than that of the typical red PH emitter tris(1-phenylisoquinolinolato-C_2, N)iridium(III) ($Ir(piq)_3$),[19] suggesting that BDBF-TP and BDBT-TP should effectively confine the triplet excitons of red PH emitters.

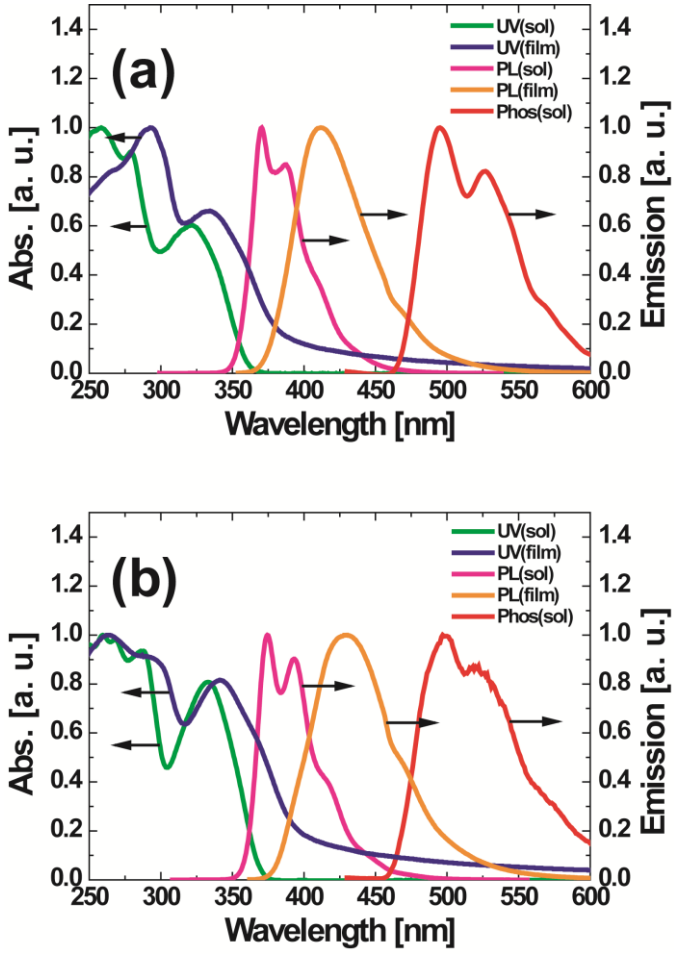

Figure 4-2. UV-vis absorption and PL spectra of (a) BDBF-TP and (b) BDBT-TP in THF solution and neat films, and corresponding phosphorescence (Phos) spectra recorded in THF at 77 K.

Figure 4-3 shows molecular structures of BDBF-TP and BDBT-TP and the distributions of their HOMOs and LUMOs obtained by DFT (B3LYP/6-31G) calculations. They have similar distributions of HOMOs and LUMOs.

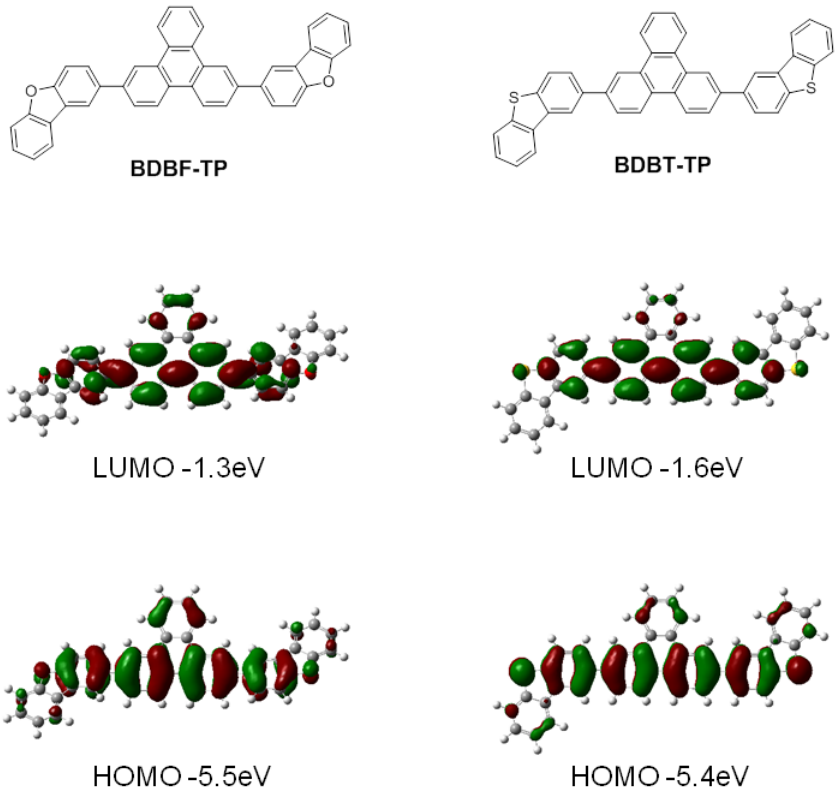

Figure 4-3. Molecular structures of BDBF-TP and BDBT-TP and the distributions of their HOMOs and LUMOs obtained by DFT (B3LYP/6-31G) calculations.

Next, unipolar carrier transport HODs and EODs were fabricated to compare the carrier transport properties of the PH host materials.[20,21] HODs with the structure of ITO/9,9',9"-triphenyl-9H,9'H,9"H-3,3':6',3"-tercarbazole (Tris-PCz) (20 nm)/PH host (60 nm)/Tris-PCz (20 nm)/LiF (1 nm)/Al (70 nm) were fabricated to compare the hole transport properties of PH hosts CBP (Device 1), BDBF-TP (Device 2) and BDBT-TP (Device 3) (Fig.

4-4 (a)). Tris-PCz was used as an electron blocking layer because it has a high-lying LUMO level (-1.9 eV). The driving voltage of Device 3 with BDBT-TP was significantly lower than those of Devices 1 and 2, indicating that BDBT-TP exhibits better hole transport properties than CBP and BDBF-TP.

EODs with the structure of ITO/BCP (20 nm)/PH host (60 nm)/BCP (20 nm)/LiF (1 nm)/Al (70 nm) were fabricated to compare the electron transport properties of PH hosts CBP (Device 1), BDBF-TP (Device 2) and BDBT-TP (Device 3) (Fig. 4-4 (b)). BCP was used as a hole blocking layer because it has a low-lying HOMO level (-6.7 eV). The lowest driving voltage was obtained for Device 3, indicating that BDBT-TP has better electron transport properties than CBP and BDBF-TP. Overall, BDBT-TP exhibits the best bipolar carrier transport properties out of BDBT-TP, CBP and BDBF-TP. The higher carrier mobilities for BDBT-TP should be attributed to more effective intermolecular π-overlap in the layer by n-σ* orbital interaction between chalcogen (S) atoms. [22-24]

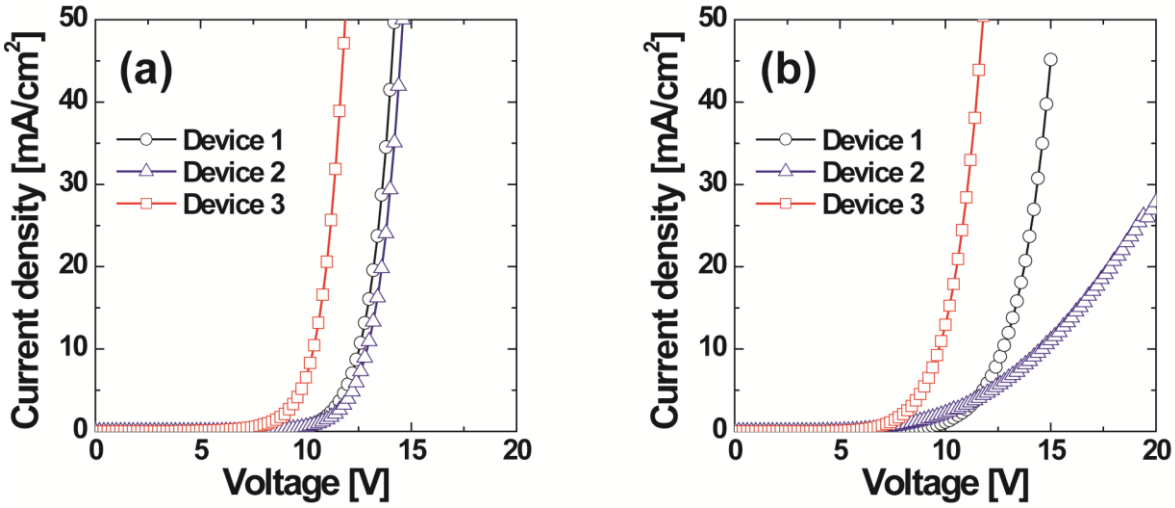

Figure 4-4. *J-V* characteristics of (a) HODs and (b) EODs.

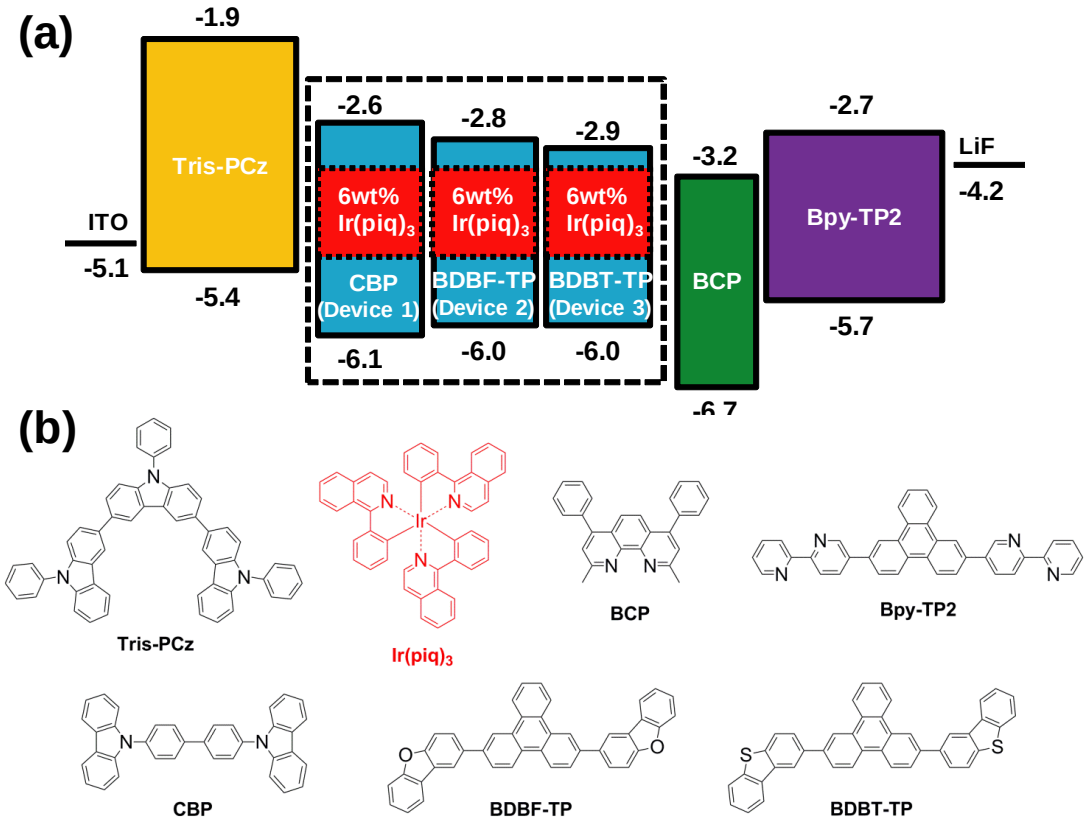

Figure 4-5. (a) Energy diagram of organic layers and (b) molecular structures of materials used in the red PHOLEDs.

To evaluate the performance of each host, red PHOLEDs[25] containing CBP (Device 1), BDBF-TP (Device 2) and BDBT-TP (Device 3) as PH hosts were fabricated (Fig. 4-5). Tris-PCz was used as a hole transport and an electron blocking layers, BCP as a hole blocking layer, 2,7-Bis(2,2'-bipyridine-5-yl)triphenylene (Bpy-TP2)[16] as an ETL and $Ir(piq)_3$ as a red emitter. If it is supposed that the carrier balance and recombination rate in the EML are both 100% and the out-coupling efficiency is 25%, the maximum η_{ext} should be about 16% for these device structures because the PL quantum yield (Φ_{PL}) of a doped film of $Ir(piq)_3$ is (57~65)±1%. The EL spectra, *J-V-L* characteristics and η_{ext} of the red PHOLEDs are shown in Fig. 4-6. All devices exhibited similar spectra with λ_{max}=625 nm (Fig. 4-6 (a)). Under a

constant current density of J=10 mA/cm^2, the driving voltages of Devices 1, 2 and 3 were 7.8, 6.4 and 7.2 V, respectively, so the driving voltages of Devices 2 and 3 were lower than that of Device 1 (Fig. 4-6 (b)). The maximum η_{ext} of Devices 1, 2 and 3 were 11.5, 12.7 and 13.6%, respectively, and 7.9, 9.1 and 12.3%, respectively, at 10 mA/cm^2 (Fig. 4-6 (c)). Device 3 with BDBT-TP as a host exhibited the highest η_{ext}. This is because of the improved carrier balance in the EML caused by more efficient bipolar carrier transport in BDBT-TP (Fig. 4-4). Moreover, the efficiency roll-off at high current density was significantly suppressed in Device 3 compared with those in Devices 1 and 2. It is believed that the difference of efficiency roll-off at high current density is related to the width and position of the recombination zone. It is inferred that Device 3 has a broader recombination zone than those of Devices 1 and 2. Although the recombination zone is primarily located near the interface with the ETL, it probably extends further into the EML in Device 3 than in Devices 1 and 2 because of the improved bipolar carrier transport in this device. Conversely, the local increase of triplet exciton density accelerates TTA or triplet exciton-polaron quenching in Devices 1 and 2 because their recombination zones are located closer to the ETL and narrower than that of Device 3.

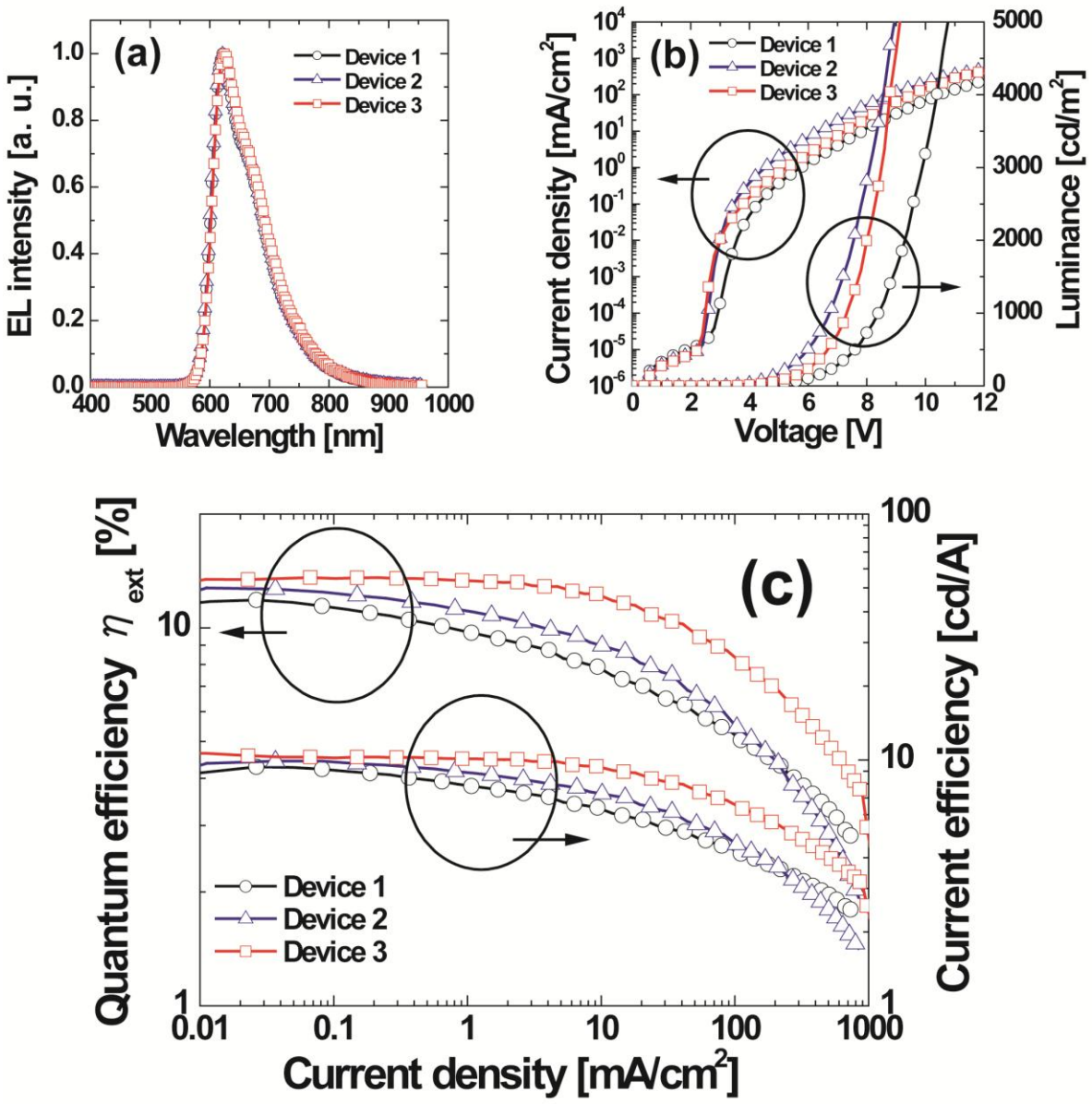

Figure 4-6. (a) EL spectra, (b) *J-V-L* characteristics and (c) η_{ext} and current efficiency against *J* for red PHOLEDs. Details of device structure are shown in Fig. 4-5.

4-4. Conclusions

I developed a novel high performance red PH host. It has better bipolar carrier transport properties in addition to a higher T_g and E_a compared with those of conventional PH hosts such as CBP and mCP. Further, it contributed to the lower driving voltage, higher η_{ext} and the suppression of efficiency roll-off at high current density in red PHOLEDs, indicating that it is a promising material as a host in practical PHOLEDs.

Finally, I look to the future development of PH host materials. Since a triphenylene backbone structure allows introduction of various substituent groups into the 2 or 11 positions, we can synthesize further derivatives as a new PH host material as shown Fig. 4-7.

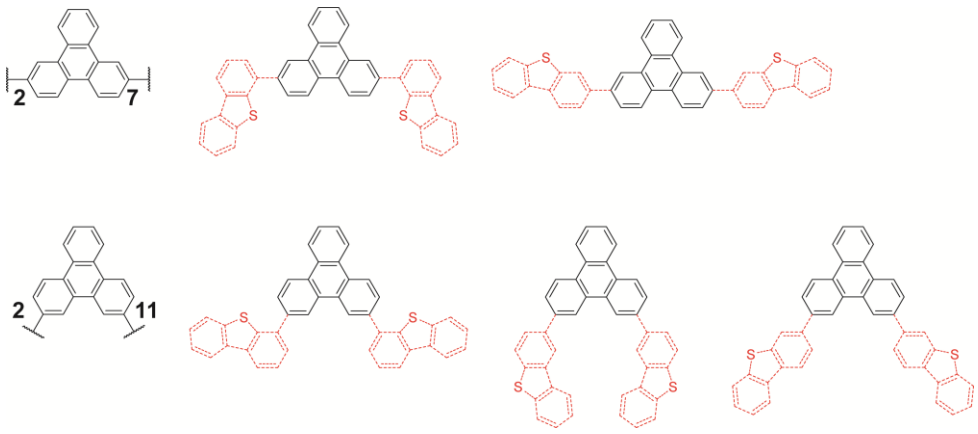

Figure 4-7. Future molecular design images of PH hosts.

4-5. References

1 C. Adachi, M. A. Baldo, M. E. Thompson and S. R. Forrest, *J. Appl. Phys.*, **2001**, 90, 5048.

2 M. A. Baldo, C. Adachi and S. R. Forrest, *Phys. Rev. B: Condens. Matter.*, **2000**, 62, 10967.

3 C. Adachi, R. Kwong and S. R. Forrest, *Org. Electron.*, **2001**, 2, 37.

4 S. Reineke, K. Walzer and K. Leo, *Phys. Rev. B: Condens. Matter. Mater. Phys.*, **2007**, 75, 125328.

5 G. He, M. Pfeiffer and K. Leo, *Appl. Phys. Lett*., **2004**, 85, 3911.

6 J. Lee, J.-I. Lee, J. Y. Lee and H. Y. Chu, *Appl. Phys. Lett*., **2009**, 94, 193305.

7 S.-J. Su, H. Sasabe, T. Takeda and J. Kido, *Chem. Mater.*, **2008**, 20, 1691.

8 Y. Tao, Q. Wang, C. Yang, Q. Wang, Z. Zhang, T. Zou, J. Qin and D. Ma, *Angew. Chem. Int. Ed.*, **2008**, 47, 8104.

9 H.-H. Chou and C.-H. Cheng, *Adv. Mater.*, **2010**, 22, 2468.

10 M.-H. Tsai, Y.-H. Hong, C.-H. Chang, H.-C. Su, C.-C. Wu, A. Matoliukstyte, J. Simokaitiene, S. Grigalevicius, J. V. Grazulevicius and C.-P. Hsu, *Adv. Mater.*, **2007**, 19, 862.

11 S.-J. Yeh, M.-F. Wu, C.-T. Chen, Y.-H. Song, Y. Chi, M.-H. Ho, S.-F. Hsu and C. H. Chen, *Adv. Mater.*, **2005**, 17, 285.

12 C.-L. Ho, W.-Y. Wong, Z.-Q. Gao, C.-H. Chen, K.-W. Cheah, B. Yao, Z. Xie, Q. Wang, D. Ma, L. Wang, X.-M. Yu, H.-S. Kwok and Z. Lin, *Adv. Funct. Mater.*, **2008**, 18, 319.

13 N. Miyaura, T. Yanagi and A. Suzuki, *Synth. Commun.*, **1981**, 11, 513.

14 W.-C. Shieh and J. A. Carlson, *J. Org. Chem.*, **1992**, 57, 379.

15 W. Li, J. Li, Y. Wu, J. Wu, R. Hotchandani, K. Cunningham, I. McFadyen, J. Bard, P. Morgan, F. Schlerman, X. Xu, S. Tam, S. J. Goldman, C. Williams, J. Sypek and T. S. Mansour, *J. Med. Chem.*, **2009**, 52, 1799.

16 K. Togashi, S. Nomura, N. Yokoyama, T. Yasuda and C. Adachi, *J. Mater. Chem.*, **2012**, 22, 20689.

17 D. Adam, P. Schuhmacher, J. Simmerer, L. Häussling, K. Siemensmeyer, K. H. Etzbach, H. Ringsdorf and D. Haarer, *Nature*, **1994**, 371, 141.

18 H. Sasabe, E. Gonmori, T. Chiba, Y.-J. Li, D. Tanaka, S.-J. Su, T. Takeda, Y.-J. Pu, K. Nakayama and J. Kido, *Chem. Mater.*, **2008**, 20, 5951.

19 A. Tsuboyama, H. Iwawaki, M. Furugori, T. Mukaide, J. Kamatani, S. Igawa, T. Moriyama, S. Miura, T. Takiguchi, S. Okada, M. Hoshino and K. Ueno, *J. Am. Chem. Soc*, **2003**, 125, 12971.

20 Y.-M. Chen, W.-Y. Hung, H.-W. You, A. Chaskar, H.-C. Ting, H.-F. Chen, K.-T. Wong and Y.-H. Liu, *J. Mater. Chem.*, **2011**, 21, 14971.

21 H.-F. Chen, T.-C. Wang, W.-Y. Hung, H.-C. Chiu, C. Yun and K.-T. Wong, *J. Mater. Chem.*, **2012**, 22, 9658.

22 K. Kobayashi, H. Masu, A. Shuto and K. Yamaguchi, *Chem. Mater.*, **2005**, 17, 6666.

23 K. Kobayashi, R. Shimaoka, M. Kawahata, M. Yamanaka and K. Yamaguchi, *Org. Lett.*, **2006**, 8, 2385.

24 Y. S. Yang, T. Yasuda and C. Adachi, *Bull. Chem. Soc. Jpn.*, **2012**, 85, 1186.

25 J. Kwak, Y.-Y. Lyu, H. Lee, B. Choi, K. Char and C. Lee, *J. Mater. Chem.*, **2012**, 22, 6351.

Chapter 5

Summary

In *Chapter 2*, the triphenylene-based ETMs, Bpy-TP1-4, were designed and synthesized for use in OLEDs. Although these materials have no T_g, they can form amorphous thin films with low surface roughness. Bpy-TP1, Bpy-TP2 and Bpy-TP4 exhibited optical anisotropy, i.e., almost parallel orientation to a substrate. Green OLEDs containing these ETMs operated at lower driving voltages than OLEDs with Alq_3. In particular, the OLED containing Bpy-TP2 showed a significantly lower driving voltage than the OLED with Alq_3. Further, Bpy-TP2 is also useful as an ETL in blue OLEDs. In comparison with the conventional ETMs, Alq_3 and TPBi, Bpy-TP2 demonstrated a lower power consumption in the device as shown in the following table. Also, the lifetime of the blue OLED containing Bpy-TP2 is equivalent to that of an OLED with TPBi. The increase in the driving voltage of the device containing Bpy-TP2 is significantly suppressed compared to that of the device with TPBi.

Blue OLED characteristics at 10 mA/cm^2

ETL	Voltage [V]	η_{ext} [%]	η_{PE} [lm/W]
Alq_3	4.5	3.7	4.4
TPBi	4.1	4.6	5.9
Bpy-TP2	3.3	4.0	6.4

Device architectures; ITO/HAT-CN (5 nm)/TPD15 (45 nm)/Tris-PCz : 4wt%DPAVBi (10 nm)/TBADN : 4wt%DPAVBi (30 nm)/ETL (30 nm)/LiF (0.5 nm)/Al (120 nm).

In *Chapter 3*, the triphenylene-based ETMs, 2,3′-Bpy-TP and 2,4′-Bpy-TP, with a coplanar and long rod-like molecular structure and a large E_a were designed and synthesized. Spectroscopic ellipsometry measurements clarified that deposited thin films of these ETMs possess larger optical anisotropy than that of 2,2′-Bpy-TP (Bpy-TP2), although they have a molecular structure similar to 2,2′-Bpy-TP, indicating that the molecules in the deposited thin films tend to almost orient horizontally to a substrate. Thus, I demonstrated that the

substitution of end groups greatly affected horizontal orientation. Furthermore, the *J-V* characteristics of EODs revealed that 2,3′-Bpy-TP and 2,4′-Bpy-TP exhibited better electron transport properties than 2,2′-Bpy-TP and the driving voltage decreased with increasing the degree of horizontal orientation of the deposited molecules. However, I demonstrated that the driving voltage decreased independent on a value of orientation parameter S in OLEDs. Therefore, it is suggested that factors other than the horizontal orientation of ETM contributes to the improvement of the *J-V* characteristics in OLEDs. Especially, it is inferred that electron injection from ETL to EML is an important factor. Therefore, in order to pull out the high electron transport properties of 2,3′-Bpy-TP and 2,4′-Bpy-TP, combining them with the EML having a lower-lying LUMO can be efficient because 2,3′-Bpy-TP and 2,4′-Bpy-TP have a low-lying LUMO level (-3.2 eV). I summarized OLED characteristics in the following table.

OLED characteristics at 10 mA/cm^2

ETL	Voltage [V]	η_{ext} [%]	η_{PE} [lm/W]
Alq_3	5.9	0.9	1.5
2,2′-Bpy-TP	4.5	1.1	2.4
2,3′-Bpy-TP	4.6	1.4	2.9
2,4′-Bpy-TP	4.8	1.0	2.0

Device architectures; ITO/α-NPD (50 nm)/Alq_3 (20 nm)/ETL (30 nm)/MgAg (100 nm)/Al (10 nm).

In *Chapter 4*, the triphenylene-based red PH host materials BDBF-TP and BDBT-TP, with high T_g (>100 ºC) and E_T (2.5 eV), were synthesized. The *J-V* characteristics of HODs and EODs showed that BDBT-TP exhibits better bipolar carrier transport properties than CBP and BDBF-TP. Red PHOLEDs containing BDBF-TP or BDBT-TP as a host showed lower driving voltage and higher η_{ext} than that containing CBP. I summarized red PH OLED characteristics in the following table. Moreover, the red PHOLED containing BDBT-TP

showed improved suppression of efficiency roll-off at high current density than those of devices containing CBP and BDBF-TP.

Red PH OLED characteristics at 10 mA/cm^2

PH host	Voltage [V]	η_{ext} [%]	η_{PE} [lm/W]
CBP	7.8	7.9	2.5
BDBF-TP	6.4	9.1	3.6
BDBT-TP	7.2	12.3	4.0

Device architectures; ITO/Tris-PCz (50 nm)/PH host : 6wt%Ir(piq)$_3$ (20 nm)/BCP (10 nm)/Bpy-TP2 (60 nm)/LiF (1 nm)/Al (70 nm).

Publication lists

Original papers

1) Kazunori Togashi, Shintaro Nomura, Norimasa Yokoyama, Takuma Yasuda and Chihaya Adachi

   Low Driving Voltage Characteristics of Triphenylene Derivatives as Electron Transport Materials in Organic Light-Emitting Diodes

   Journal of Materials Chemistry, **2012**, 22, 20689.

2) Kazunori Togashi, Takuma Yasuda and Chihaya Adachi

   Triphenylene-Based Host Materials for Low-Voltage and Highly Efficient Red Phosphorescent Organic Light-Emitting Diodes

   (*Chemistry Letters*, Accepted)

Acknowledgements

I would like to gratefully acknowledge Prof. Chihaya Adachi for many helpful discussions and enlightening suggestions. I am grateful to Prof. Totaro Imasaka and Prof. Hiroyuki Furuta for invaluable discussions and advices. I would also like to acknowledge Associate Prof. Takuma Yasuda and Assistant Prof. Kenichi Goushi who gave me invaluable comments. I am also indebted to Norimasa Yokoyama of Hodogaya Chemical Co., Ltd. for valuable suggestions and warm encouragements. I would also like to thank Shintaro Nomura and Yuta Sagara for their experimental support. Grateful thanks are also extended to the following colleagues for their stimulating discussions: Dr. Takeshi Komino, Dr. Katsuyuki Shizu, Dr. Hiroyuki Tanaka, Kensuke Masui (Fujifilm Co., Ltd.), Kuniaki Endo (Mitsubishi Rayon Co., Ltd.), Takehiro Takahashi (Hodogaya Chemical Co., Ltd.), Masaki Numata, Yu Seok Yang, Jun Yun Kim, Woong Shin, Sae Youn Lee, Jun Seong Park, Hisashi Genjima, Keiro Nasu, Ryosuke Kondo, Issei Ohtani, Hiroyuki Mieno and Takuro Nishimoto. Finally, I would also like to express my gratitude to my wife and family for their moral support and warm encouragements.